Neuron

Article

Dynorphin modulates reward-seeking actions through a pallido-amygdala cholinergic circuit

Highlights

- Dynorphin released from NAc^{Pdyn} neurons promotes VP cholinergic neuron disinhibition
- Dynorphin released from NAc^{Pdyn} neurons gates their own output via autoinhibition
- These functions are mediated by KORs on VP GABAergic neurons and NAc^{Pdyn} neurons
- Acetylcholine released from the VP into the BLA invigorates reward-seeking actions

Authors

Qingtao Sun, Mingzhe Liu, Wuqiang Guan, ..., Yulong Li, Lin Tian, Bo Li

Correspondence

qsun@cshl.edu

In brief

Sun et al. show that dynorphin released from nucleus accumbens dynorphinergic neurons potently promotes the activity of ventral pallidum cholinergic neurons via a disinhibitory circuit, thereby controlling cholinergic transmission to the amygdala. The acetylcholine released from ventral pallidum cholinergic neurons into the amygdala both facilitates learning and invigorates reward-seeking behavior.

Sun et al., 2025, Neuron *113*, 1823–1840
June 4, 2025
https://doi.org/10.1016/j.neuron.2025.03.018

CellPress

Neuron

CellPress

Article

Dynorphin modulates reward-seeking actions through a pallido-amygdala cholinergic circuit

Qingtao Sun,[1,10,11,*] Mingzhe Liu,[1,10] Wuqiang Guan,[1] Xiong Xiao,[1,2] Chunyang Dong,[3,4] Michael R. Bruchas,[5] Larry S. Zweifel,[6] Yulong Li,[7] Lin Tian,[3,8] and Bo Li[1,9]

[1]Cold Spring Harbor Laboratory, Cold Spring Harbor, NY 11724, USA
[2]Institute of Neuroscience, Key Laboratory of Brain Cognition and Brain-inspired Intelligence Technology, CAS Center for Excellence in Brain Science and Intelligence Technology, Chinese Academy of Sciences, Shanghai 200031, China
[3]Department of Biochemistry and Molecular Medicine, School of Medicine, University of California, Davis, Davis, CA, USA
[4]Department of Psychiatry and Behavioral Sciences, Stanford University, Stanford, CA, USA
[5]Department of Anesthesiology & Pain Medicine, University of Washington, Seattle, WA 98195, USA
[6]Department of Psychiatry and Behavioral Sciences, University of Washington, Seattle, WA 98195, USA
[7]State Key Laboratory of Membrane Biology, School of Life Sciences, Peking University, Beijing 100871, China
[8]Max Planck Florida Institute for Neuroscience, Jupiter, FL, USA
[9]Present address: Westlake Laboratory of Life Sciences and Biomedicine, School of Life Sciences, Westlake University, Institute of Biology, Westlake Institute for Advanced Study, Hangzhou 310024, Zhejiang, China
[10]These authors contributed equally
[11]Lead contact
*Correspondence: qsun@cshl.edu
https://doi.org/10.1016/j.neuron.2025.03.018

SUMMARY

The endogenous opioid peptide dynorphin and its receptor κ-opioid receptor (KOR) have been implicated in divergent behaviors, but the underlying mechanisms remain elusive. Here, we show that dynorphin released from nucleus accumbens dynorphinergic neurons exerts powerful modulation over a ventral pallidum (VP) disinhibitory circuit, thereby controlling cholinergic transmission to the amygdala and reward-seeking behavior in mice. On one hand, dynorphin acts postsynaptically via KORs on VP GABAergic neurons to promote disinhibition of cholinergic neurons, which release acetylcholine into the amygdala to facilitate learning and invigorate actions. On the other hand, dynorphin also acts presynaptically via KORs on dynorphinergic terminals to limit its own release. Such autoinhibition keeps cholinergic neurons from prolonged activation and release of acetylcholine and prevents perseverant reward seeking. Our study reveals how dynorphin exquisitely modulates behavior through the cholinergic system and provides an explanation for why these neuromodulators are involved in motivational disorders, including depression and addiction.

INTRODUCTION

Dynorphin is generated from the precursor protein prodynorphin (Pdyn).[1,2] It acts primarily through κ-opioid receptors (KORs), a $G_{i/o}$ type of G-protein-coupled receptor (GPCR) whose activation in general causes neuronal inhibition.[3] The inhibitory effects mediated by KORs have mostly been studied at presynaptic terminals, where activation of KORs causes suppression of neurotransmitter release. For example, in the nucleus accumbens (NAc), the bed nucleus of stria terminalis (BNST), and other brain areas, pharmacologic activation of KORs on presynaptic terminals of various types of inputs—dopaminergic, serotoninergic, GABAergic, and glutamatergic—leads to inhibition of their release of the respective neurotransmitters.[4–7] Notably, the dynorphin-/KOR-signaling-mediated presynaptic inhibition, including that observed in the NAc and BNST, is typically accompanied by strong aversive or anxiogenic effects,[3,7–10] which have led to the prevailing view that dynorphin and KORs form an "anti-reward" system in the brain.[3,11,12]

However, dynorphin/KOR signaling is also involved in reward-seeking behaviors through, at least in part, modulation of hypothalamic neurons,[13–17] and recent studies show that stimulation of Pdyn neurons, which presumably induces dynorphin release, in the dorsal striatum[18] or a subpopulation of Pdyn neurons in the NAc[19,20] drives potent appetitive responses and positive reinforcement. These findings indicate that dynorphin/KOR signaling is more complicated than being simply anti-reward and raise the possibility that the behavioral roles of this signaling may depend upon its actions in specific brain areas or the specific neural circuits therein.

Pdyn neurons in the NAc (NAc^{Pdyn} neurons) are the major source of dynorphin production in the brain.[8] Apart from local

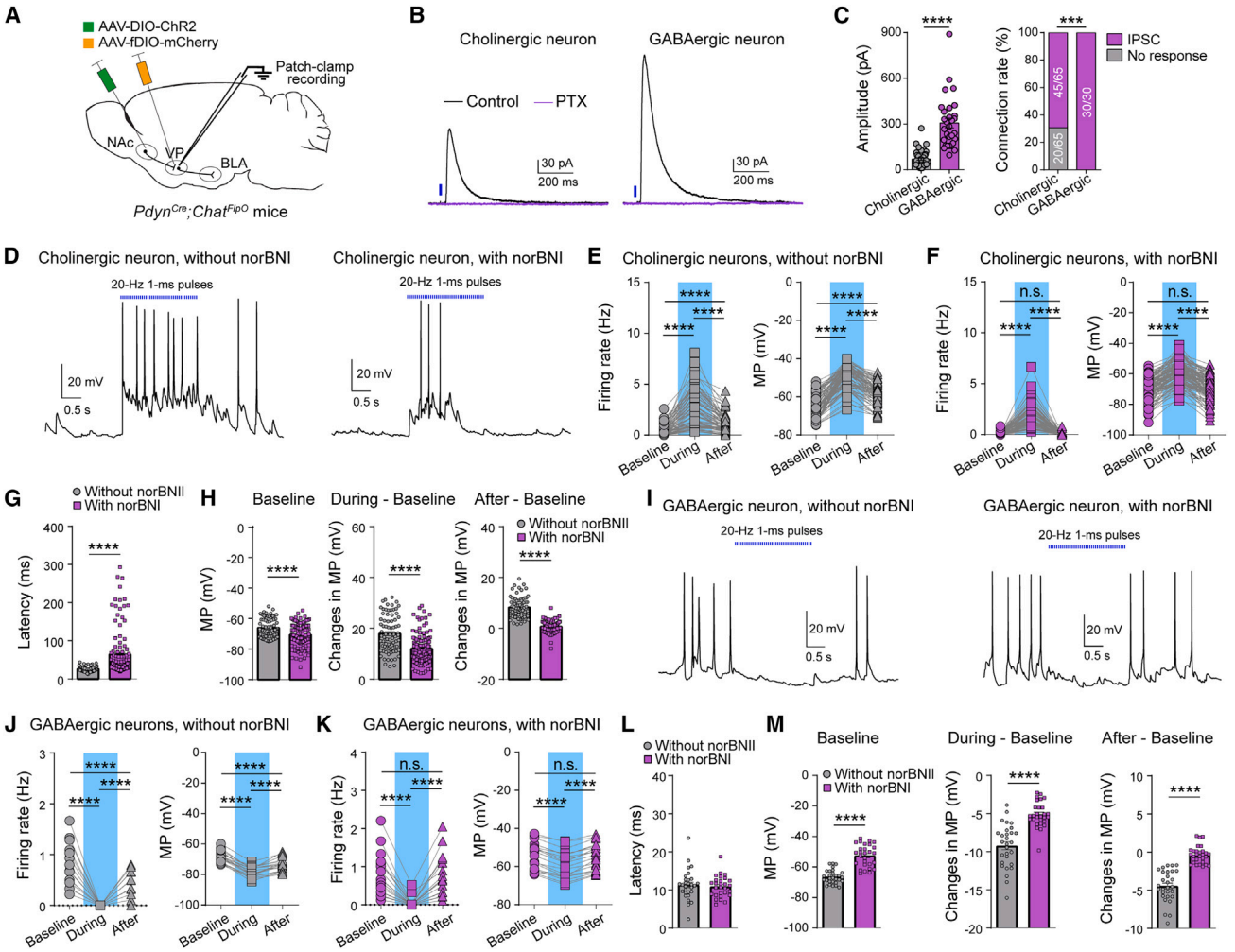

Figure 1. NAc^{Pdyn} neurons drive disinhibition of VP^{ChAT} neurons in a dynorphin-/KOR-signaling-dependent manner

(A) A schematic of the approach. NAc, nucleus accumbens; VP, ventral pallidum; BLA, basolateral amygdala.

(B) Traces of IPSCs recorded from a cholinergic neuron (left) and an adjacent putative GABAergic neuron (right) in the VP in the same slice in response to photo-stimulation of axon terminals originating from NAc^{Pdyn} neurons. PTX, picrotoxin.

(C) Quantification of IPSC amplitude (left) and connection rate (right) of cholinergic (mCherry^{+}) and putative GABAergic (mCherry^{-}) neurons (data were obtained from 7 mice; amplitude: cholinergic, $n = 45/65$ neurons, GABAergic, $n = 30/30$ neurons, Mann-Whitney test, $^{****}p < 0.0001$; connection rate, cholinergic, 45 out of 65 neurons had measurable IPSCs, GABAergic, 30 out of 30 neurons had measurable IPSCs, chi-squared test, $^{***}p = 0.0006$). Connection rate is calculated as the ratio of neurons exhibiting measurable light-evoked IPSCs among all recorded neurons.

(D) Traces of current-clamp recording from cholinergic neurons in response to photo-stimulation of axon terminals originating from NAc^{Pdyn} neurons. Left: without norBNI; right: with norBNI (100 nM).

(E) Quantification of firing rate (left) and membrane potential (MP, right) before, during, and after the photo-stimulation in the absence of norBNI ($n = 79$ neurons from 7 mice; firing rate, $^{****}p < 0.0001$; MP, $^{****}p < 0.0001$; Wilcoxon signed-rank test).

(F) Same as (E) except that recording was performed in the presence of norBNI ($n = 117$ neurons from 7 mice; firing rate, $^{****}p < 0.0001$; n.s., nonsignificant, $p = 0.5345$; MP, $^{****}p < 0.0001$; n.s., $p = 0.5519$; Wilcoxon signed-rank test).

(G) Quantification of the latency of light-evoked firing (without norBNI, $n = 79$ neurons from 7 mice; with norBNI, $n = 117$ neurons from 7 mice; $^{****}p < 0.0001$, Mann-Whitney test).

(H) Quantification of baseline MP (left), changes in MP from baseline to photo-stimulation period (middle), and changes in MP from baseline to after photo-stimulation period (right) ($^{****}p < 0.0001$, Mann-Whitney test).

(I) Traces of current-clamp recording from putative GABAergic neurons in response to photo-stimulation of axon terminals originating from NAc^{Pdyn} neurons. Left: without norBNI; right: with norBNI (100 nM).

(J) Quantification of firing rate (left) and MP (right) before, during, and after the photo-stimulation in the absence of norBNI ($n = 29$ neurons from 3 mice; firing rate, $^{****}p < 0.0001$; MP, $^{****}p < 0.0001$; Wilcoxon signed-rank test).

(K) Same as (J), except that recording was performed in the presence of norBNI ($n = 28$ neurons from 3 mice; firing rate, $^{****}p < 0.0001$; n.s., $p = 0.2126$; MP, $^{****}p < 0.0001$; n.s., $p = 0.0726$; Wilcoxon signed-rank test).

(legend continued on next page)

release of dynorphin within the NAc—where it may exert its anti-reward function by, for example, presynaptic inhibition of dopaminergic inputs from the ventral tegmental area (VTA)[5,21] or glutamatergic inputs from the amygdala[4]—in principle, dynorphin should also be released by NAc^{Pdyn} neurons into downstream brain regions through their long-range projections. The ventral pallidum (VP; also known as substantia innominata) is the major output structure of the NAc[22] and is a key structure involved in goal-directed motivation, including the motivation to pursue appetitive stimuli and the motivation to avoid aversive stimuli.[23–27] In particular, recent studies demonstrate that different types of neurons in the VP—including cholinergic, GABAergic, and glutamatergic neurons—have distinct roles in learning or invigorating valence-specific behaviors.[13,27–33] Whether and how NAc^{Pdyn} neurons and their release of dynorphin participate in regulating VP neurons, thereby influencing motivated behaviors, remain unknown and warrant careful study.

Here, we investigated the roles of dynorphin/KOR signaling from NAc^{Pdyn}→VP projections in regulating VP neuronal function and motivated behavior. Through molecular, genetic, and optogenetic manipulations, in combination with electrophysiology, *in vivo* real-time recording of dynorphin release in behaving animals, and behavioral characterization, we uncover that dynorphin released from NAc^{Pdyn} neurons powerfully controls a disinhibitory circuit in the VP via both postsynaptic KORs on local GABAergic neurons and presynaptic KORs on NAc^{Pdyn} axon terminals. Through this mechanism, dynorphin promotes and, furthermore, fine-tunes the activation of VP cholinergic neurons and their release of acetylcholine (ACh) into the basolateral amygdala (BLA), which, in turn, both facilitates learning and invigorates reward-seeking actions.

RESULTS

NAc^{Pdyn} neurons are the major source of NAc outputs to the VP

Previous studies indicate that NAc^{Pdyn} neurons belong to dopamine receptor D1 (Drd1) type of medium spiny neurons.[19,20] Because Drd1 neurons are heterogeneous,[18] we characterized them with single-molecule fluorescent *in situ* hybridization (smFISH). These neurons are composed of two major populations, with one expressing *Pdyn* and the other expressing *Tshz1* (Figures S1A–S1D), akin to the Drd1 neurons in the dorsal striatum.[18] To examine the connectivity between these neurons and neurons in the VP, the major target of the NAc, we performed retrograde mono-transsynaptic tracing with rabies virus (RV), using VP neurons expressing either glutamate decarboxylase 2 (Gad2, a marker for GABAergic neurons) or choline acetyltransferase (ChAT, a marker for cholinergic neurons) as the starter cells (Figure S2A; STAR Methods). We subsequently used smFISH to identify the types of RV-labeled neurons. For both classes of starter cells, most of the RV-labeled neurons in the NAc expressed *Pdyn* (Figures S2B–S2E; Gad2, 73%, ChAT, 82%). To verify the cell types directly innervated by NAc^{Pdyn} neurons, we performed anterograde mono-transsynaptic tracing with an herpes simplex virus (HSV) strain, using NAc^{Pdyn} neurons as the starter cells (Figure S2F). Subsequent smFISH revealed that the HSV-labeled neurons in the VP included both GABAergic neurons and cholinergic neurons, with GABAergic neurons being the majority (Figures S2G–S2K). In addition, we examined the axon fibers originating from NAc^{Pdyn} neurons (Figure S2L). These neurons send dense projections to the VP, spanning its anterior and posterior domains; they also send projections to the nucleus basalis of Meynert (NBM) but send very few to no projections to the horizontal limb of the diagonal band (HDB). These results indicate that NAc^{Pdyn} neurons provide the major source of NAc outputs to VP neurons.

NAc^{Pdyn} neurons disinhibit VP cholinergic neurons in a KOR-dependent manner

To examine the functional impact of NAc^{Pdyn} neuron outputs on VP neurons, we used *Pdyn^{Cre};ChAT^{FlpO}* mice in which we injected the NAc and VP, respectively, with an adeno-associated virus (AAV) expressing the light-gated cation channel Channelrhodopsin (ChR2) in a Cre-dependent manner (AAV-DIO-ChR2) and an AAV expressing a red fluorescent protein mCherry in a Flp-dependent manner (AAV-fDIO-mCherry) (Figure 1A). This strategy allowed selective expression of ChR2 in NAc^{Pdyn} neurons and mCherry in VP ChAT-expressing (VP^{ChAT}) and thus cholinergic neurons. Acute slices containing the VP were prepared from these mice. We photo-stimulated axon fibers originating from NAc^{Pdyn} neurons and recorded the evoked inhibitory postsynaptic currents (eIPSCs) from mCherry-positive (mCherry^{+}) VP^{ChAT} neurons as well as adjacent mCherry-negative (mCherry^{-}) neurons in the same slices (Figure 1B). The latter population should mostly be GABAergic neurons, as they are the predominant neuron type in the VP.[27] Notably, VP^{ChAT} neurons exhibited much smaller $GABA_A$-mediated eIPSCs and lower probability of exhibiting such eIPSCs than the putative GABAergic neurons (Figures 1B and 1C). These results show that NAc^{Pdyn} neurons make stronger inhibitory synapses and have higher synaptic connectivity with GABAergic neurons than cholinergic neurons in the VP, and suggest that NAc^{Pdyn} neurons may drive disinhibition of the cholinergic neurons.

To test this possibility, we recorded the firing and membrane potential of VP^{ChAT} neurons in response to optogenetic stimulation of NAc^{Pdyn} terminals. Strikingly, the stimulation induced a marked increase in neuronal firing and depolarization, which lasted for seconds after cessation of the photo-stimulation (Figures 1D–1F). We reasoned that the lasting disinhibition is mediated by dynorphin signaling, which is slower than $GABA_A$-mediated fast synaptic transmission. Indeed, application of KOR antagonist norbinaltorphimine (norBNI) decreased the resting membrane potential, decreased the light-evoked firing

(L) Quantification of the latency of light-evoked firing (without norBNI, n = 29 neurons from 3 mice; with norBNI, n = 28 neurons from 3 mice; p = 0.7097, Mann-Whitney test).

(M) Quantification of baseline MP (left), changes in MP from baseline to photo-stimulation period (middle), and changes in MP from baseline to after photo-stimulation period (right) (without norBNI, n = 29 neurons from 7 mice; with norBNI, n = 28 neurons from 7 mice; ****$p < 0.0001$, Mann-Whitney test). Data are presented as mean ± SEM.

and depolarization, increased the latency of the firing, and completely blocked the lasting disinhibition of VP^{ChAT} neurons (Figures 1D–1H). These results suggest that dynorphin signaling makes an important contribution to the disinhibition of VP cholinergic neurons, including the slower, lasting component of the disinhibition.

Correspondingly, optogenetic stimulation of NAc^{Pdyn} terminals led to a dramatic decrease in firing and hyperpolarization of the putative VP GABAergic neurons (Figures 1I–1K), which lasted beyond the duration of photo-stimulation. These inhibitory effects were diminished by norBNI (Figures 1I–1M). These results together suggest that NAc^{Pdyn} neurons drive disinhibition of VP cholinergic neurons by inhibiting local GABAergic neurons in a manner that depends on dynorphin/KOR signaling.

KORs on GABAergic neurons are required for the disinhibition

To verify whether KORs on local GABAergic neurons contribute to the disinhibition of VP^{ChAT} neurons, we repeated the above experiments in $Gad2^{Cre}$ mice in which *Oprk1* expression in VP GABAergic (VP^{GABA}) neurons was selectively suppressed using CRISPR-Cas9-mediated mutagenesis. To this end, we used our recently developed AAV that conditionally expresses SaCas9 and a single-guide RNA targeting *Oprk1* (AAV1-FLEX-SaCas9-U6-sgOprk1).[34] An AAV with the same design but expressing a guide RNA that targets Rosa26 (AAV1-FLEX-SaCas9-U6-sgRosa26) was used as a control.[34] We confirmed that expressing sg*Oprk1* in VP^{GABA} neurons led to effective suppression of *Oprk1* (Figure S3). For the electrophysiology experiment, we used $Gad2^{Cre}$;$ChAT^{FlpO}$ mice and injected the VP with the AAV that expresses sgOprk1, or the control sgRosa26, in a Cre-dependent (and thus GABAergic-neuron-specific) manner, together with the AAV that expresses mCherry in a Flp-dependent (and thus cholinergic-neuron-specific) manner (Figure S4A). In addition, we injected the NAc of the same mice with the Cre-dependent AAV to express ChR2 in GABAergic neurons, including NAc^{Pdyn} neurons.

We obtained whole-cell patch-clamp recording from $mCherry^+$ VP^{ChAT} neurons in acute slices. In the sgRosa26 control group, photo-stimulation (2 s, 20 Hz) of $ChR2^+$ fibers originating from the NAc successfully induced disinhibition of VP^{ChAT} neurons, which lasted beyond the cessation of light (Figures S4B–S4D). Administration of norBNI substantially reduced the disinhibition during photo-stimulation and completely abolished the disinhibition after the cessation of light. By contrast, in the sgOprk1 group, the photo-stimulation-induced disinhibition of VP^{ChAT} neurons was much reduced and did not last beyond the cessation of light (Figures S4E–S4G). Application of norBNI did not further diminish the disinhibition, suggesting an occlusion effect (Figures S4E–S4I). These results indicate that KORs on local GABAergic neurons play a critical role in mediating the disinhibition of VP cholinergic neurons driven by NAc inputs.

NAc^{Pdyn} neurons modulate reward-induced ACh release in the BLA

To investigate the *in vivo* function of NAc^{Pdyn}-neuron-driven disinhibition of VP cholinergic neurons, we virally expressed ChR2 in NAc^{Pdyn} neurons and the ACh sensor gACh3.0[35] in the BLA (Figure 2A), one of the major targets of VP cholinergic neurons[28,33,36,37] (Figure S5). Optical fibers were implanted above the NAc and the BLA for photo-stimulation and photometry, respectively (Figures S6A and S6B). Remarkably, a single pulse of blue light delivered to the NAc with a duration as short as 50 ms was sufficient to trigger a robust gACh3.0 response in the BLA (Figures 2B and S6C). Furthermore, photo-activation of the axon fibers in the VP originating from NAc^{Pdyn} neurons similarly triggered gACh3.0 response in the BLA (Figures 2C, 2D and S6D–S6F). By contrast, optogenetically activating Tshz1 or dopamine receptor D2 (Drd2) neurons in the NAc (targeted with $Tshz1^{Cre}$ or *Adora2a-Cre* mice, respectively) (Figures S7A–S7H), or activating the projections from hypothalamic Pdyn neurons to the VP (Figures S7I–S7N), failed to induce any gACh3.0 response in the BLA. Interestingly, all these manipulations caused place aversion in a real-time place preference or aversion (RTPP/A) test (Figures S7O–S7Q), an effect that is opposite to activating NAc^{Pdyn} neurons[19,20] (also see results below in Figure S13). These results suggest that NAc^{Pdyn} neurons have a specific role in driving disinhibition of VP cholinergic neurons, leading to ACh release in the BLA.

Next, we tested whether NAc^{Pdyn} neurons are required for ACh release in the BLA. We expressed the light-sensitive proton pump archaerhodopsin (ArchT) or mCherry (as a control) in NAc^{Pdyn} neurons and expressed gACh3.0 in BLA neurons. Optical fibers were implanted above the infected areas in the NAc and BLA for light inhibition and photometry, respectively (Figures 2E, S8A, and S8B). The mice were water restricted and presented with two stimuli that were either rewarding or aversive: water and air-puff blowing to the face, respectively (Figure 2E). In randomly interleaved trials, we delivered brief (150 ms) green light pulses to the NAc during the water or air-puff presentations. Both water and air-puff triggered robust gACh3.0 response in the BLA (Figures 2F, 2G, S8C, and S8D). Interestingly, the water-evoked response, but not the air-puff-evoked response, in the ArchT mice was consistently reduced by the light pulses (Figures 2F, 2G, and S8C). In the mCherry mice, neither response was affected by the light pulses (Figures 2H, 2I, and S8D). These results suggest that inhibition of NAc^{Pdyn} neurons selectively impairs reward-evoked ACh release in the BLA.

To determine whether this effect is mediated by the NAc→VP pathway, we expressed parapinopsin (PPO), an opsin that causes rapid and sustained inhibition of presynaptic release upon blue light illumination,[38] in NAc^{Pdyn} neurons (Figures 2J, S8E, and S8F). The mice were presented with water and air-puff as described above. In interleaved trials, we delivered blue light (10 mW, 10 s) into the VP to inhibit the NAc^{Pdyn} terminals before water or air-puff presentations (Figure 2J; STAR Methods). The light delivery substantially decreased gACh3.0 response to water but did not affect that to air-puff (Figures 2K, 2L, and S8G). In mCherry control mice, light delivery into the VP had no effect on either the water-evoked or the air-puff-evoked gACh3.0 response (Figures 2M, 2N, and S8H). In addition, in mice expressing a mutant form of the gACh3.0 in the BLA that is insensitive to ACh (gACh3.0-mut),[35] no response can be detected in the BLA when the mice were presented with

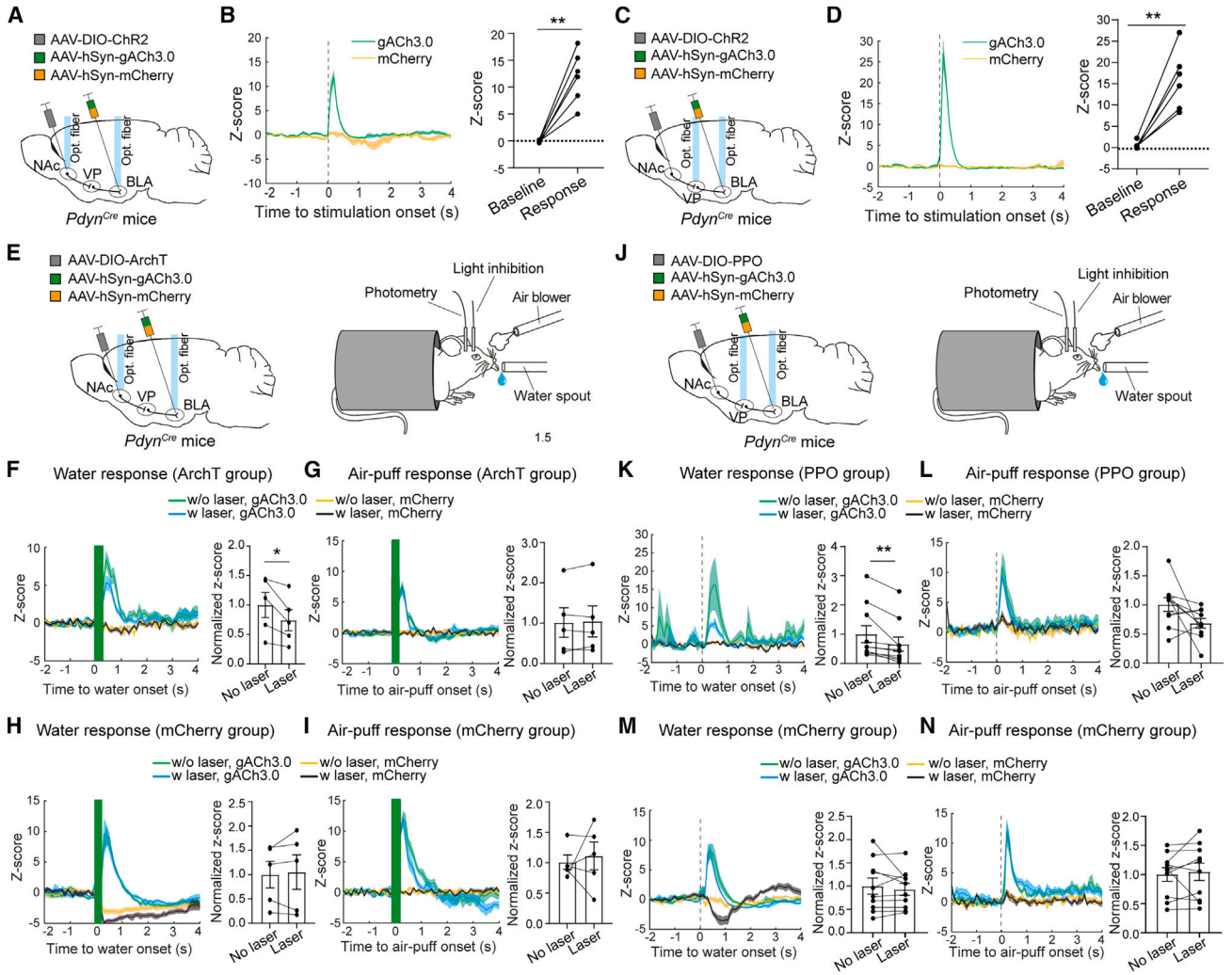

Figure 2. NAc^{Pdyn}→VP projections modulate ACh release in the BLA

(A) A schematic of the approach.

(B) Left: average gACh3.0 signals from a mouse that received photo-stimulation in the NAc. mCherry signals are also shown to monitor potential motion artifacts. Right: quantification of the photo-stimulation-evoked response for all mice (n = 6 mice, t = 6.34, $^{**}p$ = 0.0014, paired t test).

(C) A schematic of the approach.

(D) Left: average gACh3.0 signals from a mouse that received photo-stimulation in the VP. mCherry signals are also shown to monitor potential motion artifacts. Right: quantification of the photo-stimulation-evoked response for all mice (n = 6 mice, t = 5.86, $^{**}p$ = 0.0021, paired t test).

(E) Schematics of the approach (left) and experimental design (right).

(F) Left: average gACh3.0 signals from an ArchT mouse that received water. mCherry signals are also shown to monitor potential motion artifacts. Right: quantification of the response to water for all mice (n = 5 mice, t = 3.09, $^{*}p$ = 0.0366, paired t test).

(G) Same as (F), except that the mice received air-puff and the response was to air-puff (n = 5 mice, t = 0.56, p = 0.6, paired t test).

(H) Left: average gACh3.0 signals from an mCherry mouse that received water. mCherry signals are also shown to monitor potential motion artifacts. Right: quantification of the response to water for all mice (n = 5 mice, t = 0.54, p = 0.62, paired t test).

(I) Same as (H), except that the mice received air-puff and the response was to air-puff (n = 5 mice, t = 0.42, p = 0.69, paired t test).

(J) Schematics of the approach (left) and experimental design (right).

(K) Left: average gACh3.0 signals from a PPO mouse that received water. mCherry signals are also shown to monitor potential motion artifacts. Right: quantification of the response to water for all mice (n = 10 mice, t = 3.51, $^{**}p$ = 0.0067, paired t test).

(L) Same as (K), except that the mice received air-puff and the response was to air-puff (n = 10 mice, t = 2.12, p = 0.0631, paired t test).

(M) Left: average gACh3.0 signals from an mCherry mouse that received water. mCherry signals are also shown to monitor potential motion artifacts. Right: quantification of the response to water for all mice (n = 10 mice, t = 0.74, p = 0.48, paired t test).

(N) Same as (M), except that the mice received air-puff and the response was to air-puff (n = 10 mice, t = 0.5, p = 0.63, paired t test). Data are presented as mean ± SEM.

either water reward or air-puff (Figures S8I–S8K), validating the authenticity of the signals. Together, these results indicate that NAc^{Pdyn} neurons specifically regulate reward-induced ACh release in the BLA through the NAc→VP pathway.

NAc^{Pdyn}→VP projections control reward-seeking behavior

To examine the behavioral role of the NAc→VP pathway, we sought to optogenetically manipulate NAc^{Pdyn}→VP projections in mice during motivated behaviors. We first infected NAc^{Pdyn} neurons bilaterally with the AAV expressing PPO or mCherry and implanted optical fibers above the VP for light delivery (Figures 3A and 3B). These mice were trained in a go/no-go task, where two different tones (the conditioned stimuli [CS]) predicted the delivery of either water or air-puff (the unconditioned stimuli [US]) (Figures 3B and 3C; STAR Methods). During training, a blue light covering the time window between CS onset and US onset was delivered into the VP. Strikingly, compared with the control group, the PPO group had much reduced anticipatory licking in both the go and the no-go trials, resulting in a reduced hit rate but increased correct rejection rate (CR) throughout training (Figures 3D–3G). The overall performance of the PPO group was impaired, mainly because of the large reduction in hit rate (Figure 3G). These results suggest that inhibition of NAc^{Pdyn} axon terminals in the VP leads to impaired learning and/or motor functions. To disentangle these possibilities, we gave the animals additional training in the absence of the blue light until the PPO group fully learned the task (i.e., reached a success rate of at least 80%; STAR Methods). We then tested these mice again in the go/no-go task, where the same blue light stimulation was delivered into the VP in randomly interleaved trials (STAR Methods). Light inhibition of the NAc^{Pdyn}→VP pathway after learning did not affect the performance or the licking behavior of the animals (Figures S9A–S9D). These results suggest that the NAc^{Pdyn}→VP pathway is likely required for learning of the go/no-go task. By contrast, it is not essential for execution of the task in well-trained mice nor is it essential for the motor program underlying licking behavior.

We next infected NAc^{Pdyn} neurons bilaterally with the AAV expressing ChR2 or mCherry and implanted optical fibers above the VP for light delivery (Figures 3A and 3B). These mice were also trained in the go/no-go task in which a train of blue light pulses covering the time window between CS onset and US onset was delivered into the VP (Figures 3B and 3C; STAR Methods). Compared with the control group, the ChR2 group had much enhanced anticipatory licking in both the go and the no-go trials, resulting in an increased hit rate but reduced CR throughout training (Figures 3H–3K). The overall performance of the ChR2 group was impaired, mainly because of the large reduction in CR (Figure 3K). Again, we gave the animals additional training in the absence of the blue light until the ChR2 group reach a level of performance comparable with the control group (i.e., reached a success rate of at least 80%; STAR Methods). We subsequently retested these mice in the go/no-go task in which the blue light was delivered into the VP in randomly interleaved trials (STAR Methods). The light stimulation still dramatically decreased the CR and increased licking of the ChR2 mice during no-go trials (Figures S9E–S9H), similar to the effect during learning (Figures 3H–3K). It did not appreciably affect the hit rate and licking of these mice in go trials, likely because of a ceiling effect.

To further verify whether the NAc^{Pdyn}→VP pathway might directly control the motor program underlying licking, we tested mice that had learned to lick a water spout to obtain water (STAR Methods). Delivering blue light pulses into the VP readily triggered licking responses in the ChR2 mice (but not in the control mice) when they were thirsty (Figure S9I). However, when the same ChR2 mice were sated on water, the light could no longer elicit licking (Figure S9J). In another cohort of mice that had never been exposed to a water spout, light activation of the NAc^{Pdyn}→VP pathway did not induce any licking (Figure S9K). Moreover, light inhibition or activation of the NAc^{Pdyn}→VP pathway did not appreciably influence the locomotion of mice in an open field (Figures S9L–S9N). These results together suggest that the NAc^{Pdyn}→VP projections have an important role in learning in the go/no-go task and appear to have an additional role in promoting reward-seeking behavior. However, this pathway does not directly control motor functions.

Reward induces dynorphin release in the VP

Our results from *ex vivo* brain slices suggest that dynorphin/KOR signaling makes an important contribution to the disinhibition of VP cholinergic neurons driven by NAc^{Pdyn}→VP projections (Figures 1 and S4), whereas those from *in vivo* optogenetics suggest that these projections control reward-seeking behavior (Figures 3 and S9). However, how endogenous dynorphin participates in modulating VP function and animal behavior is poorly understood, as *in vivo* real-time measurement of dynorphin dynamics has been infeasible until recently.[39] To address this issue, we infected VP neurons with our recently developed genetically encoded dynorphin sensor kLight1.3[39] and implanted an optical fiber above the infected area for recording kLight1.3 signals with photometry (Figures 4A and S10A). Again, the mice were presented with water and air-puff, as described above (Figure 2E). Notably, water evoked a clear increase in kLight1.3 signals, whereas air-puff caused a decrease in the signals (Figures 4B and 4C).

We repeated the above experiments in *Pdyn* conditional knockout ($Pdyn^{flox/flox}$) mice[40] in which *Pdyn* was deleted in NAc neurons by an AAV expressing Cre, resulting in $NAc^{Pdyn-/-}$ mice (Figures 4A–4C). The deletion of *Pdyn*, which was confirmed with smFISH (Figures S10B–S10D), markedly decreased water- or air-puff-evoked kLight1.3 signals in the VP of these mice as compared with the signals from their wild-type control ($NAc^{Pdyn+/+}$) mice (Figures 4B and 4C), indicating that the kLight1.3 signals represent dynorphin released by NAc^{Pdyn} neurons. These results demonstrate that a naturally rewarding stimulus triggers endogenous dynorphin release from NAc^{Pdyn} neurons into the VP.

Dynorphin modulates ACh release in the BLA and reward-seeking actions in mice

To determine the *in vivo* function of dynorphin released by NAc^{Pdyn} neurons, we first asked whether it is required for ACh release in the BLA. We deleted *Pdyn* in NAc neurons as described

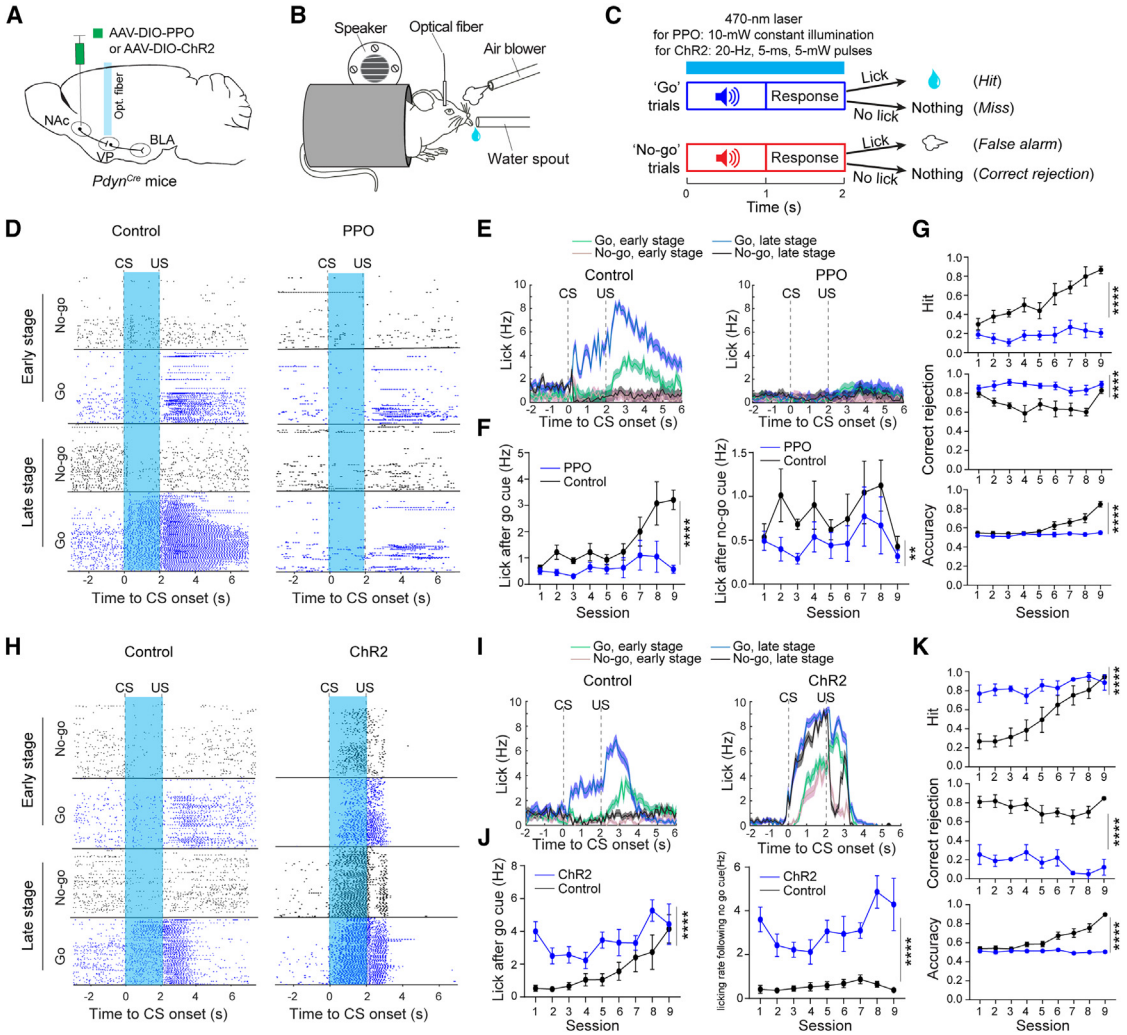

Figure 3. NAc^{Pdyn}→VP projections regulate reward-seeking behavior

(A–C) Schematics of the approach (A), experimental setup (B), and task design (C).

(D) Lick raster of an mCherry control mouse (left) and a PPO mouse (right) during go/no-go training. The blue shaded area indicates the time window when the laser was turned on.

(E) Average licking rates of the same mice in (D).

(F) Left: quantification of licking rates following CS onset in go trials across training sessions ($F(1,81) = 31.49$, $^{****}p = 2.7 \times 10^{-7}$). Right: licking rates following CS onset in no-go trials across training sessions ($F(1,81) = 8.679$, $^{**}p = 0.0042$). PPO group, $n = 6$ mice, mCherry group, $n = 5$ mice, two-way ANOVA followed by Sidak's test.

(G) Top: hit rate, $F(1,81) = 142$, $^{****}p < 1 \times 10^{-15}$. Middle: CR rate, $F(1,81) = 74.96$, $^{****}p = 3.77 \times 10^{-13}$. Bottom: accuracy, $F(1,81) = 71.78$, $^{****}p = 8.78 \times 10^{-13}$. PPO group, $n = 6$ mice, mCherry group, $n = 5$ mice, two-way ANOVA followed by Sidak's test.

(H) Lick raster of an mCherry mouse (left) and a ChR2 mouse (right) during go/no-go training. The blue shaded area indicates the time window when the laser was turned on.

(I) Average licking rates of the same mice in (H).

(J) Left: quantification of licking rates following CS onset in go trials across training sessions ($F(1,81) = 35.25$, $^{****}p = 7 \times 10^{-8}$). Right: licking rate following CS onset in no-go trials across training sessions ($F(1,81) = 110.4$, $^{****}p < 1 \times 10^{-15}$). ChR2 group, $n = 6$ mice, mCherry group, $n = 5$ mice, two-way ANOVA followed by Sidak's test.

(K) Top: hit rate, $F(1,81) = 67.66$, $^{****}p = 2.7 \times 10^{-12}$. Middle: CR rate, $F(1,81) = 332.3$, $^{****}p < 1 \times 10^{-15}$. Bottom: accuracy, $F(1,81) = 189.1$, $^{****}p < 1 \times 10^{-15}$. ChR2 group, $n = 6$ mice, mCherry group, $n = 5$ mice. Two-way ANOVA followed by Sidak's test. Data are presented as mean ± SEM.

above and simultaneously expressed ChR2 in these neurons (Figures 4D, S10E, and S10F). The ACh sensor, gACh3.0, was expressed in the BLA of the same mice. Brief light pulses delivered to the NAc only triggered modest gACh3.0 responses in the BLA of these NAc$^{Pdyn-/-}$ mice, which were much smaller than the responses in NAc$^{Pdyn+/+}$ mice (Figures 4E and 4F). This result suggests that dynorphin released from NAc^{Pdyn} neurons is needed for effective ACh release in the BLA.

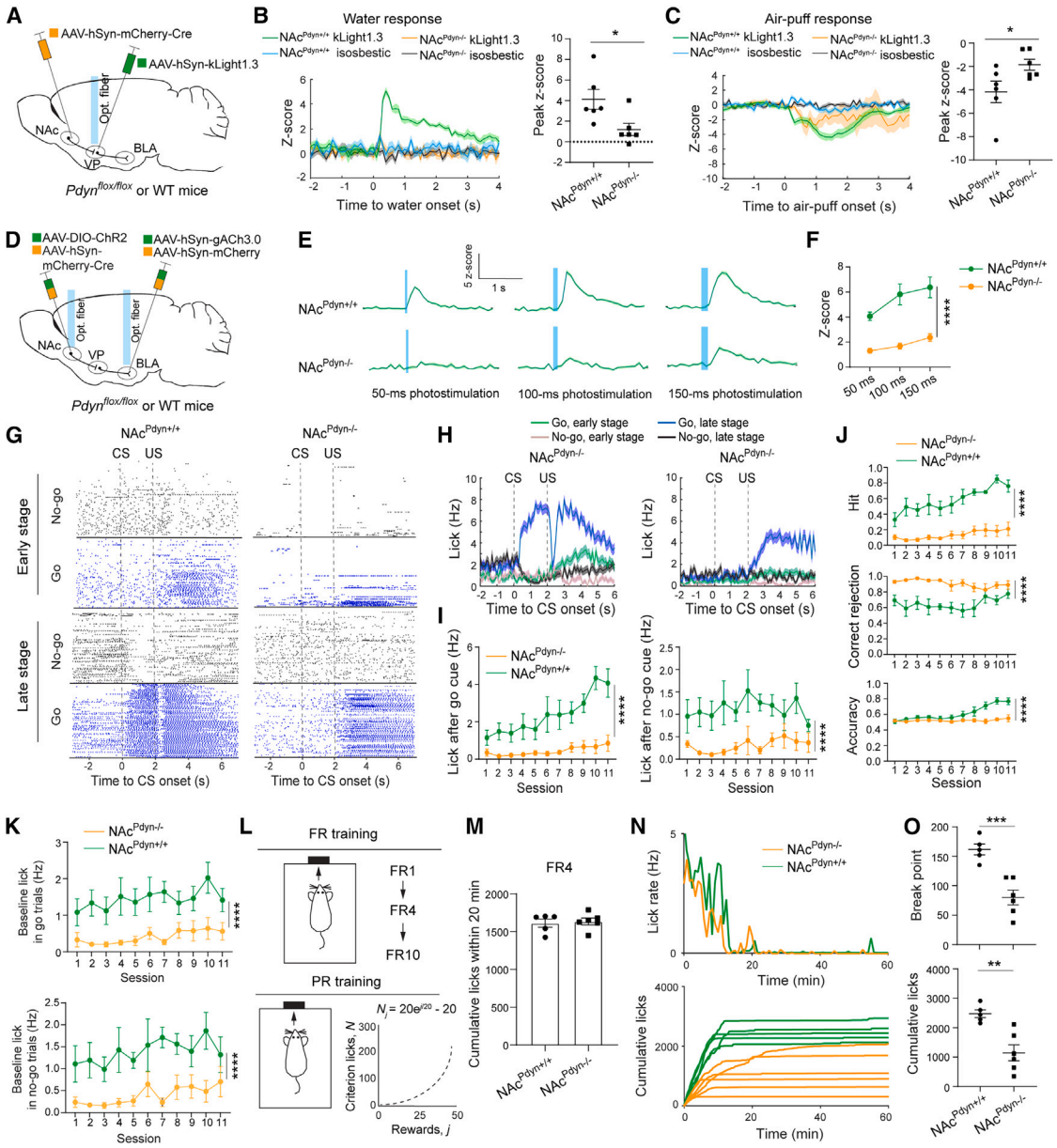

Figure 4. Dynorphin release into the VP is required for acetylcholine release in the BLA and reward-seeking actions in mice

(A) A schematic of the approach.

(B) Left, average klight1.3 signals in the VP of a NAc$^{Pdyn+/+}$ mouse and a NAc$^{Pdyn-/-}$ mouse that received water. Signals from the isosbestic channel are also shown to monitor potential motion artifacts. Right, quantification of the response to water for all mice (n = 6 mice in each group, t = 2.59, *p = 0.027, unpaired t test).

(C) Left, average klight1.3 signals in the VP of a NAc$^{Pdyn+/+}$ mouse and a NAc$^{Pdyn-/-}$ mouse that received air-puff. Signals from the isosbestic channel are also shown to monitor potential motion artifacts. Right, quantification of the response to air-puff for all mice (n = 6 mice in each group, t = 2.25, *p = 0.0478, unpaired t test).

(D) A schematic of the approach.

(E) Average gACh3.0 signals in the BLA of a NAc$^{Pdyn+/+}$ mouse (upper) and a NAc$^{Pdyn-/-}$ mouse (lower) that received photo-stimulation of NAc neurons with different durations of light pulses.

(F) Quantification of the photo-stimulation triggered response for all animals (n = 6 mice in each group, F(1,30) = 70.78, ****p = 2.17 ×10^{-9}, two-way ANOVA followed by Sidak's test).

(G) Lick raster of a NAc$^{Pdyn+/+}$ (control) mouse (left) and a NAc$^{Pdyn-/-}$ mouse (right) during go/no-go training.

(H) Average licking rates of the same mice in (G).

(legend continued on next page)

To verify this result and determine whether dynorphin acts via VP neurons, we pharmacologically blocked KOR with norBNI, applied either systemically (Figures S11A–S11P; STAR Methods) or locally within the VP (Figures S12A–S12K; STAR Methods). *Pdyn*^{Cre} mice were used in these experiments in which we measured ACh sensor gACh3.0 responses in the BLA to optogenetic activation of NAc^{Pdyn} neurons. In both cases, norBNI reduced the responses (Figures S11C, S11D, S11O, S11P, S12B, S12J, and S12K). Interestingly, systemic or local norBNI application also reduced gACh3.0 responses induced by water reward but did not affect the responses induced by air-puff (Figures S11E, S11F, S12C, and S12D). In control animals in which saline was administered in lieu of norBNI, gACh3.0 responses in the BLA were stable (Figures S11G and S11H). These results together indicate that dynorphin released from NAc^{Pdyn} neurons is required for reward-induced ACh release in the BLA, likely because dynorphin/KOR signaling is critical for the disinhibition of VP cholinergic neurons (see Figures 1 and S4).

To examine whether dynorphin released by NAc^{Pdyn} neurons is important for reward-driven behavior, we trained NAc$^{Pdyn-/-}$ and NAc$^{Pdyn+/+}$ mice in the go/no-go task (Figures 4G–4J). The NAc$^{Pdyn-/-}$ mice showed markedly lower anticipatory licking response and lower hit rate than the control mice in go trials (Figures 4G–4I). The NAc$^{Pdyn-/-}$ mice also showed a lower anticipatory licking response and therefore a higher CR rate in no-go trials. Because of the marked reduction in hit rate, the overall performance of these mice was worse than the control mice (Figure 4J). Notably, the NAc$^{Pdyn-/-}$ mice showed much reduced baseline licking activity in both go and no-go trials (Figure 4K). Consistent with these observations, the mice in which KOR was blocked by norBNI systemically or locally within the VP showed similar phenotypes (Figures S11I–S11N and S12E–S12I). Of note, the effect of norBNI is long lasting.[7,19,41]

The profound reduction in licking in the NAc$^{Pdyn-/-}$ mice throughout the go/no-go task is reminiscent of the effects of PPO inhibition of the NAc^{Pdyn}→VP projections (Figures 3D–3G), suggesting impaired learning. The results that the NAc$^{Pdyn-/-}$ mice and norBNI-treated mice had reduced baseline licking, and that activating the NAc^{Pdyn}→VP pathway promotes reward seeking in a need-dependent manner (Figures S9I–S9K), prompted us to further examine whether dynorphin/KOR signaling in this pathway has functions beyond learning. We trained NAc$^{Pdyn-/-}$ and NAc$^{Pdyn+/+}$ mice to obtain water reward in a progressive-ratio (PR) task in which they learned first that a fixed number of licks led to one reward (i.e., the reward under a fixed ratio [FR]; Figure 4L; STAR Methods). They were subsequently tested in the PR situation where the number of licks required for the animals to attain water reward increased progressively and the breakpoint at which the mice stopped responding was used as a measure of motivation.[42] There was no difference between the two groups in their licking response for reward under a FR (Figure 4M). However, the NAc$^{Pdyn-/-}$ mice showed substantially decreased breakpoint and cumulative licking for reward under the PR (Figures 4N and 4O). Thus, NAc$^{Pdyn-/-}$ mice have reduced ability to attain reward when it requires some effort, but their performance is indistinguishable from the wild types' if the task is less demanding.

Recent studies show that stimulation of Pdyn neurons in the NAc can convey valence information and drive place preference.[19,20] Therefore, we examined whether manipulations of dynorphin/KOR signaling in the NAc→VP pathway would affect behavior in the RTPP/A test. Activating NAc^{Pdyn} neurons or their projections to the VP induced robust RTPP (see all the control groups in Figures S13A–S13O), consistent with the previous studies. Interestingly, activating NAc neurons still induced robust RTPP in the NAc$^{Pdyn-/-}$ mice (Figures S13A–S13C) or in the mice in which norBNI was administered systemically (Figures S13D–S13F) or locally within the VP (Figures S13G–S13I). In fact, infusing norBNI into the VP even enhanced the RTPP (Figures S13G–S13I). These results, together with the results described in the following sections (also see Figures S13J–S13O), suggest that valence information from NAc^{Pdyn} neurons is conveyed by GABA rather than dynorphin.

Together, these results suggest that dynorphin released from the NAc^{Pdyn}→VP circuit contributes to the disinhibition of VP cholinergic neurons and their subsequent ACh release into the BLA; it also contributes not only to learning but also to promoting reward-seeking behavior in situations where the reward can only be achieved after significant effort investment.

KORs on VP GABAergic neurons are required for ACh release and motivated behavior

We reasoned that KORs on VP GABAergic neurons are involved in the modulation of ACh release in the BLA and animal behavior. To test this, we again used the AAV1-FLEX-SaCas9-U6-sg*Oprk1* to suppress *Oprk1* in VP GABAergic neurons (see Figure S3). In the BLA of the same mice, we expressed gACh3.0 and implanted optical fibers for recording ACh release with photometry (Figures 5A and S14A–S14C). Similar to treatment with norBNI (Figures S11E–S11H, S12C, and S12D), suppressing *Oprk1* in VP GABAergic neurons reduced BLA gACh3.0 responses to water but did not affect the responses to air-puff (Figures 5B and

(I) Left: quantification of licking rates following CS onset in go trials across training sessions ($F(1,99) = 104.8$, $^{****}p < 1 \times 10^{-15}$). Right: licking rates following CS onset in no-go trials across training sessions ($F(1,99) = 60.12$, $^{****}p = 8.06 \times 10^{-13}$). NAc$^{Pdyn-/-}$ group, $n = 6$ mice, NAc$^{Pdyn+/+}$ group, $n = 5$ mice, two-way ANOVA followed by Sidak's test.

(J) Top: hit rate, $F(1,99) = 235.3$, $^{****}p < 1 \times 10^{-15}$. Middle: CR rate, $F(1,99) = 100.5$, $^{****}p < 1 \times 10^{-15}$. Bottom: accuracy, $F(1,99) = 55.52$, $^{****}p = 3.52 \times 10^{-11}$. NAc$^{Pdyn-/-}$ group, $n = 6$ mice, NAc$^{Pdyn+/+}$ group, $n = 5$ mice, two-way ANOVA followed by Sidak's test.

(K) Baseline licking rates during go/no-go training (upper: go trials, $F(1,99) = 74.72$, $^{****}p = 9.8 \times 10^{-14}$; lower: no-go trials, $F(1,99) = 63.62$, $^{****}p = 2.7 \times 10^{-12}$; two-way ANOVA followed by Sidak's test).

(L) Schematics of the design for fixed-ratio (FR) task and progressive-ratio (PR) task.

(M) Cumulative licks under FR4 in a 20-min time window ($t = 0.33$, $p = 0.75$, unpaired t test).

(N) Upper: lick rate for a NAc$^{Pdyn-/-}$ and NAc$^{Pdyn+/+}$ mouse during PR test. Lower: cumulative licks for the NAc$^{Pdyn-/-}$ and NAc$^{Pdyn+/+}$ mice during PR test.

(O) Quantification of break points (upper) and cumulative licks (lower) during PR test (break points, $t = 5.05$, $^{***}p = 0.0007$; cumulative licks, $t = 4.11$, $^{**}p = 0.0026$; NAc$^{Pdyn-/-}$ group, $n = 6$ mice, NAc$^{Pdyn+/+}$ group, $n = 5$ mice, unpaired t test). Data are presented as mean ± SEM.

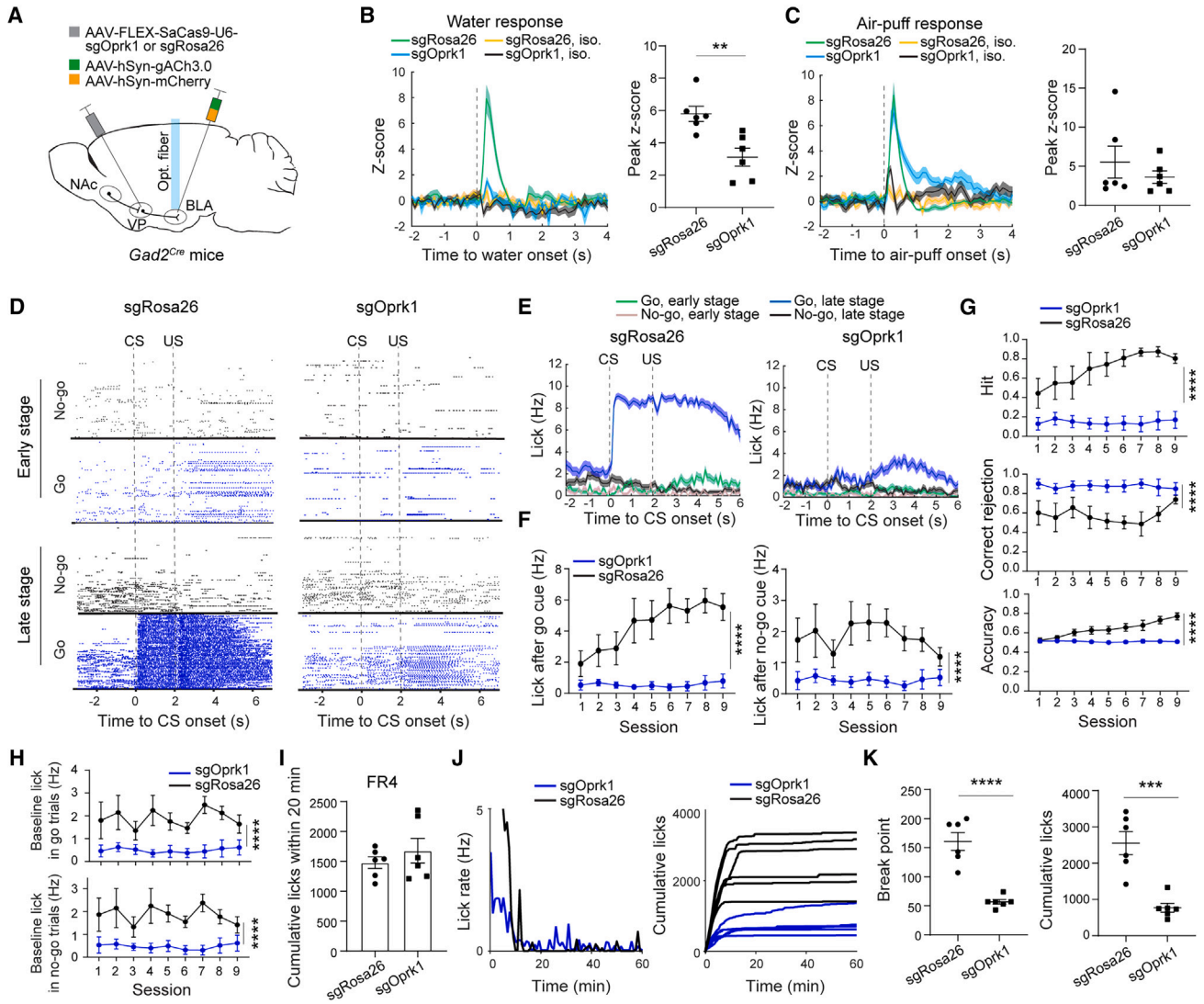

Figure 5. KORs on VP GABAergic neurons are required for acetylcholine release in the BLA and reward-seeking actions in mice

(A) A schematic of the approach.

(B) Left, average gACh3.0 signals in the BLA of an sgRosa26 (control) mouse and an sgOprk1mouse that received water. Signals from the isosbestic (iso.) channel are also shown to monitor potential motion artifacts. Right, quantification of the response to water for all mice (n = 6 mice in each group, t = 3.67, $^{**}p$ = 0.0043, unpaired t test).

(C) Average gACh3.0 signals in the BLA of an sgRosa26 (control) mouse and an sgOprk1mouse that received air-puff. Signals from the isosbestic (iso.) channel are also shown to monitor potential motion artifacts. Right, quantification of the response to air-puff for all animals (n = 6 mice in each group, t = 0.88, p = 0.4, unpaired t test).

(D) Lick raster of an sgRosa26 mouse (left) and an sgOprk1 mouse (right) during go/no-go training.

(E) Average licking rates of the same mice in (D).

(F) Left: quantification of licking rates following CS onset in go trials across training sessions (F(1,90) = 113.1, $^{****}p < 1 \times 10^{-15}$. Right: licking rates following CS onset in no-go trials across training sessions (F(1,90) = 48.94, $^{****}p = 4.53 \times 10^{-10}$. N = 6 animals in each group, two-way ANOVA followed by Sidak's test.

(G) Top: hit rate, F(1,90) = 136.3, $^{****}p < 1 \times 10^{-15}$. Middle: CR rate, F(1, 90) = 57.15, $^{****}p = 3.26 \times 10^{-11}$. Bottom: accuracy, F(1,90) = 105.6, $^{****}p < 1 \times 10^{-15}$. n = 6 animals in each group, two-way ANOVA followed by Sidak's test.

(H) Baseline licking rates during go/no-go training (upper: go trials, F(1,90) = 52.6, $^{****}p = 1.37 \times 10^{-10}$; lower: no-go trials, F(1,90) = 47.56, $^{****}p = 7.16 \times 10^{-10}$; two-way ANOVA followed by Sidak's test).

(I) Cumulative licks under FR4 in a 20-min time window (t = 0.88, p = 0.4, unpaired t test).

(J) Left: lick rate for an sgRosa26 and sgOprk1 mouse during PR test. Right: cumulative licks for the sgRosa26 and sgOprk1 mice during PR test.

(K) Quantification of break points (left) and cumulative licks (right) during PR test (break points, t = 6.53, $^{****}p$ = 0.00007; cumulative licks, t = 5.22, $^{***}p$ = 0.0004; sgOprk1 group, n = 6 mice, sgRosa26 group, n = 6 mice, unpaired t test). Data are presented as mean ± SEM.

5C). Suppressing *Oprk1* in VP GABAergic neurons also reduced anticipatory licking and performance (Figures 5D–5G and S14D), as well as baseline licking (Figure 5H) in the go/no-go task. This manipulation did not affect the behavior of animals in the elevated plus maze test (Figures S14E–S14G), suggesting that it does not affect basal anxiety levels. These results indicate that KORs on VP GABAergic neurons are required for normal ACh release in the BLA and learning in the go/no-go task, consistent with the above findings from the optogenetic, genetic, and pharmacologic manipulations of the NAc^{Pdyn}→VP pathway.

Furthermore, in the PR task, although suppressing *Oprk1* in VP GABAergic neurons had no effect on the licking response for reward under a FR (Figure 5I), it decreased breakpoint and cumulative licking for reward under the PR (Figures 5J and 5K). To further verify this finding, we tested a separate cohort of mice performing a free-moving version of the PR test, where nose pokes were required to obtain water reward (Figures S15A and S15B). Consistent with the results from the head-fixed PR task, suppressing *Oprk1* in VP GABAergic neurons did not affect the pokes under a FR (Figure S15C) but reduced breakpoint and cumulative pokes under the PR (Figures S15D–S15G). Interestingly, suppressing *Oprk1* in VP GABAergic neurons reduced the time mice spent around the water port without affecting their locomotion (Figures S15H and S15I). These results together suggest that KOR-mediated signaling in VP GABAergic neurons is critical for learning as well as for invigorating reward-seeking behaviors, likely by modulating VP cholinergic neurons and their release of ACh in the BLA.

To examine whether KORs on VP GABAergic neurons are required for valence processing, we suppressed *Oprk1* in these neurons, as above, and expressed ChR2 in GABAergic neurons in the NAc, where optical fibers were also implanted for photo-stimulation. These mice were subjected to the RTPP test, where they showed robust preference for the stimulation side, similar to control mice (Figures S13J–S13L). This result confirms the above finding that dynorphin/KOR signaling in the NAc→VP pathway is not essential for valence processing (Figures S13A–S13I).

The autoinhibitory function of KORs on NAc^{Pdyn} neurons

Previous studies show that KORs are highly expressed in Drd1 neurons in the NAc.[4] Indeed, we found that *Oprk1* is expressed in almost all NAc^{Pdyn} neurons (Figures S16A and S16B), which are the major subtype of NAc Drd1 neurons (Figure S1). Because KORs can mediate presynaptic inhibition of inhibitory synapses,[4,7] we reasoned that KORs on NAc^{Pdyn} neurons may gate the output of these neurons via autoinhibition. To test this, we injected the NAc of $Pdyn^{Cre}$ mice with the sgOprk1 (or the control sgRosa26) virus together with a ChR2 virus to infect NAc^{Pdyn} neurons. The sgOprk1 virus led to suppression of *Oprk1* in NAc^{Pdyn} neurons (Figures S16A and S16C), as expected. In the BLA of the same mice, we expressed gACh3.0. Optical fibers were implanted in the NAc and the BLA for photo-stimulation and photometry, respectively (Figures 6A and S16D).

Remarkably, the photo-stimulation-triggered gACh3.0 responses in the sgOprk1 mice lasted much longer than those in the control mice, although the response amplitude was similar between the two groups (Figures 6B and 6C). Consistently, in acute slices, the NAc^{Pdyn}-neuron-driven disinhibition of VP^{ChAT} neurons in the sgOprk1 group lasted longer than the control group (Figure S17). These results indicate that a normal function of KORs on NAc^{Pdyn} neurons is to gate the output of these neurons via autoinhibition, thereby limiting the disinhibition of VP^{ChAT} neurons and their release of ACh in the BLA.

To determine how KORs on NAc^{Pdyn} neurons might influence motivated behavior, we suppressed *Oprk1* in NAc^{Pdyn} neurons with the sgOprk1 virus and trained these animals and their controls in the go/no-go task (Figures 6D–6G). Compared with the control mice, the sgOprk1 mice showed enhanced licking in no-go trials (Figures 6D–6F), resulting in a decreased CR rate and overall performance (Figure 6G). In addition, in the PR test, the sgOprk1 mice showed markedly increased breakpoint and cumulative licking (Figures 6H–6K), albeit their licking responses under a FR remained normal (Figure 6H). These results indicate that an impairment in dynorphin/KOR signaling in NAc^{Pdyn} neurons leads to abnormally enhanced reward-seeking actions, even when there is a punishment (such as the air-puff in the no-go trials).

On the other hand, suppressing *Oprk1* in NAc^{Pdyn} neurons increased the place preference driven by photo-stimulation of NAc^{Pdyn} neurons (Figures S13M–S13O), an effect similar to that of infusing norBNI into the VP (Figures S13G–S13I). Because both manipulations reduce dynorphin/KOR signaling in the presynaptic terminals of NAc^{Pdyn} neurons, which can lead to enhanced GABA release,[4–7] it is possible that the increased place preference is caused by enhanced GABA release from these neurons.

VP cholinergic output to the BLA invigorates reward-seeking actions

Our results thus far indicate that dynorphin/KOR signaling in the NAc→VP circuit modulates VP cholinergic outputs to the BLA and plays important roles both in learning and in invigorating reward-seeking actions. It is well known that cholinergic inputs to the BLA, including those originating from the VP, have an important role in learning.[28,30,33,37,43] Could these cholinergic inputs also be involved in invigorating reward-seeking actions? To address this question, we first examined the effects of activating VP→BLA cholinergic projections. We expressed ChR2 (or yellow fluorescent protein [YFP] as a control) in VP^{ChAT} neurons in $ChAT^{FlpO}$ mice and implanted optical fibers in the BLA of the same mice for light delivery (Figures 7A and S18A–S18E). The two groups had a comparable licking response under a FR (Figure 7K, left), suggesting that both groups learned the task. These mice were subsequently tested in PR sessions, in one of which they received photo-stimulation in the BLA (see STAR Methods). We found that the photo-stimulation consistently increased the ChR2 mice's breakpoint and cumulative licking (Figures 7B and 7C), whereas it had no effect on the control mice (Figures 7D and 7E). The photo-stimulation did not induce RTPP or RTPA in these mice, although it slightly decreased their locomotion (Figures S18F and S18G). These results indicate that activating VP→BLA cholinergic projections promotes animals' reward-seeking actions.

Finally, we examined the effects of inhibiting VP→BLA cholinergic projections. We expressed PPO (or GFP, as a

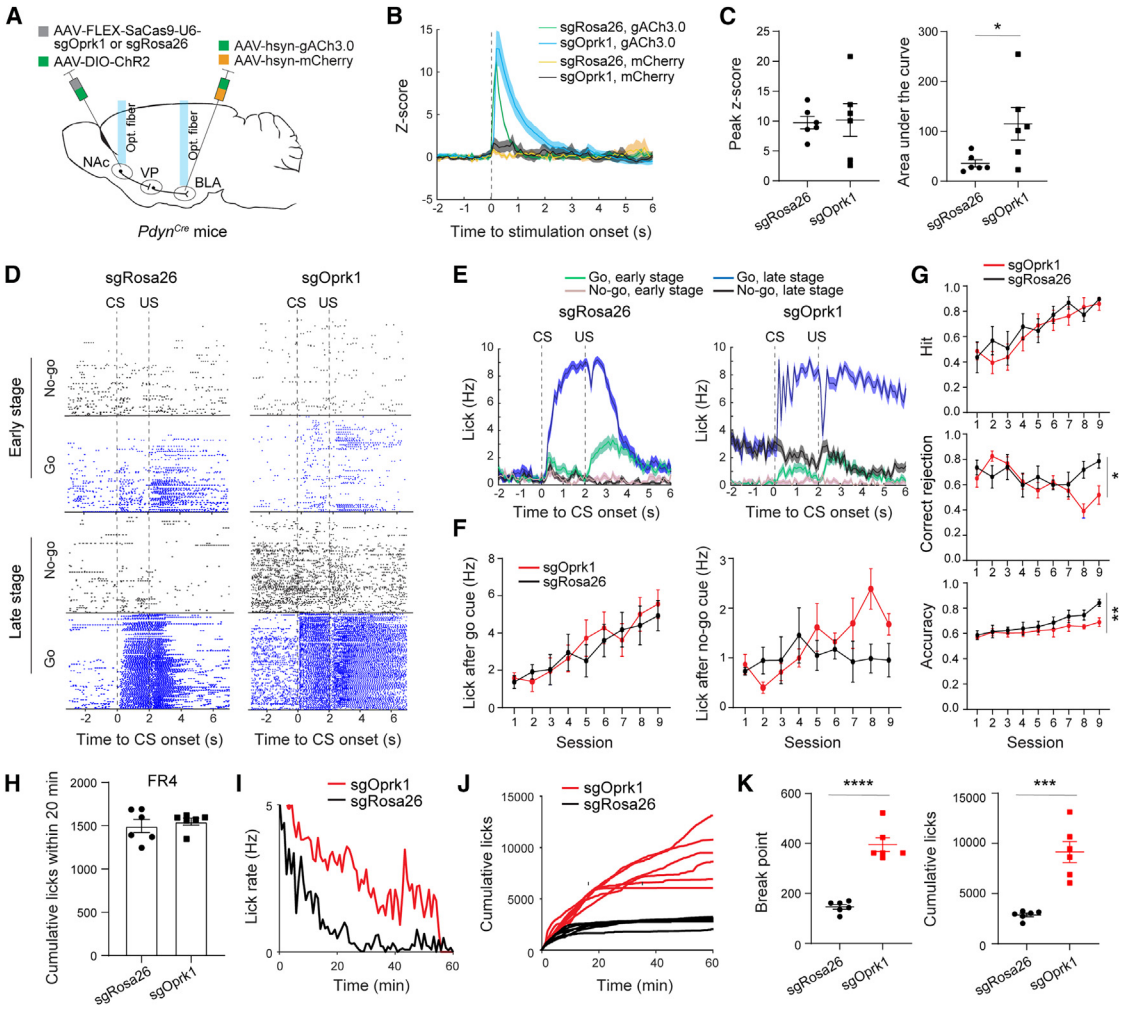

Figure 6. KORs on NAc^{Pdyn} neurons limit acetylcholine release in the BLA and reward-seeking actions in mice

(A) A schematic of the approach.

(B) Average gACh3.0 signals in the BLA of an sgRosa26 (control) mouse and an sgOprk1mouse that received photo-stimulation in the NAc. mCherry signals are used to monitor potential motion artifacts.

(C) Quantification of the photo-stimulation-evoked response for all mice. Left: amplitude, t = 0.18, $p = 0.88$; right: area under the curve, t = 2.37, $^{*}p = 0.039$; $n = 6$ mice for each group, unpaired t test.

(D) Lick raster of an sgRosa26 mouse (left) and an sgOprk1 mouse (right) during go/no-go training.

(E) Average licking rates of the same mice in (D).

(F) Left: quantification of licking rates following CS onset in go trials across training sessions, F(1,90) = 0.3026, $p = 0.5836$. Right: licking rates following CS onset in no-go trials across training sessions, F(1,90) = 3.247, $p = 0.075$. $N = 6$ animals in each group, two-way ANOVA followed by Sidak's test.

(G) Top: hit rate, F(1,90) = 1.021, $p = 0.315$. Middle: CRrate, F(1,90) = 3.968, $^{*}p = 0.049$. Bottom: accuracy, F(1,90) = 8.83, $^{**}p = 0.0038$. $N = 6$ animals in each group, two-way ANOVA followed by Sidak's test.

(H) Cumulative licks under FR4 in a 20-min time window (t = 0.58, $p = 0.57$, unpaired t test).

(I) Lick rate for an sgRosa26 and sgOprk1 mouse during PR test.

(J) Cumulative licks for the sgRosa26 and sgOprk1 mice during PR test.

(K) Quantification of break points (left) and cumulative licks (right) during PR test (break points, t = 8.54, $^{****}p = 6.58 \times 10^{-6}$; cumulative licks, t = 5.88, $^{***}p = 0.0002$; $n = 6$ mice in each group, unpaired t test). Data are presented as mean ± SEM.

control) in VP^{ChAT} neurons in *ChAT^{FlpO}* mice and implanted optical fibers in the BLA of the same mice (Figures 7F and S18H–S18J). The two groups had comparable licking responses under a FR (Figure 7K, right), suggesting that they learned the task equally well. These mice were then tested in PR sessions to evaluate the effects of photo-stimulation in the BLA (STAR Methods). Light delivery into the BLA led to a consistent decrease in breakpoint and cumulative licking in the PPO mice (Figures 7G and 7H), but it did not affect the behavior of the control mice (Figures 7I and 7J), indicating that inhibiting VP→BLA cholinergic terminals weakens animals' reward-seeking actions. These results together suggest that

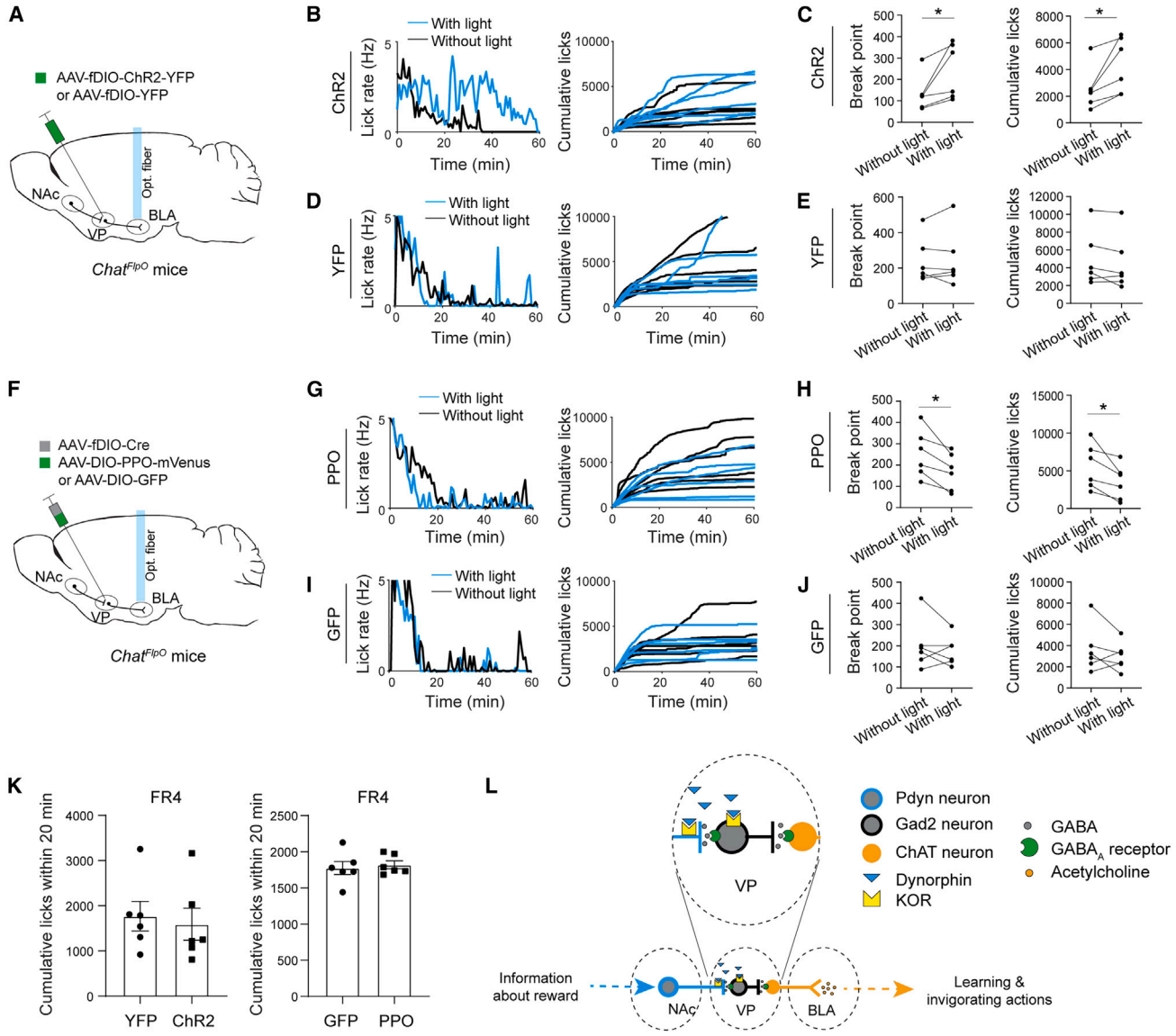

Figure 7. VP→BLA cholinergic projections modulate reward-seeking actions

(A) A schematic of the approach.

(B) Left: lick rate for a ChR2 mouse during PR test. Right: cumulative licks for the ChR2 mice during PR test.

(C) Quantification of break points (left) and cumulative licks (right) for the ChR2 mice during PR test (break points, t = 2.7, *p = 0.0428; cumulative licks, t = 3.04, *p = 0.0289; n = 6 mice in each group, unpaired t test).

(D) Left: lick rate for a YFP mouse during PR test. Right: cumulative licks for the YFP mice during PR test.

(E) Quantification of break points (left) and cumulative licks (right) for the YFP mice during PR test (break points, t = 0.3, p = 0.78; cumulative licks, t = 1.7, p = 0.15; n = 6 mice in each group, unpaired t test).

(F) A schematic of the approach.

(G) Left: lick rate for a PPO mouse during PR test. Right: cumulative licks for the PPO mice during PR test.

(H) Quantification of break points (left) and cumulative licks (right) for the PPO mice during PR test (break points, t = 3.86, *p = 0.119; cumulative licks, t = 3.2, *p = 0.0243; n = 6 mice in each group, unpaired t test).

(I) Left: lick rate for a GFP mouse during PR test. Right: cumulative licks for the GFP mice during PR test.

(J) Quantification of break points (left) and cumulative licks (right) for the GFP mice during PR test (break points, t = 0.84, p = 0.44; cumulative licks, t = 1.07, p = 0.33; n = 6 mice in each group, unpaired t test).

(K) Cumulative licks under FR4 in a 20-min time window for the mice used in (A)–(E) (left, t = 0.37, p = 0.72), and for mice used in (F)–(J) (right, t = 0.42, p = 0.68, unpaired t test).

(L) A circuit model. Inset shows an enlarged VP and its circuit elements.

Data are presented as mean ± SEM.

the cholinergic inputs from the VP to the BLA indeed have a role in invigorating reward-seeking actions.

DISCUSSION

Our results support a model in which dynorphin released by NAc^{Pdyn} neurons in response to reward powerfully modulates a disinhibitory circuit in the VP. This circuit, in turn, controls activation of cholinergic neurons and their release of ACh into the BLA, which exerts two distinct functions: facilitating learning and invigorating actions during reward-seeking behavior (model Figure 7L). In this disinhibitory circuit—which consists of the projections from NAc^{Pdyn} neurons to the VP, local VP GABAergic (VP^{GABA}) neurons, and VP cholinergic (VP^{ChAT}) neurons projecting to the BLA—activation of NAc^{Pdyn} neurons causes potent and lasting inhibition of VP^{GABA} neurons and disinhibition of VP^{ChAT} neurons, leading to robust ACh release into the BLA. These processes appear to be critical for both learning and invigorating reward-seeking actions. In particular, dynorphin release by NAc^{Pdyn} neurons, which occurs in response to reward delivery, plays an indispensable and intricate role in these processes. The released dynorphin acts through KORs in two locations within this circuit: VP^{GABA} neurons and NAc^{Pdyn} projections to the VP, which are postsynaptic and presynaptic, respectively, with respect to the site of dynorphin production (Figure 7L). Through activation of KORs on VP^{GABA} neurons, dynorphin enables potent and lasting inhibition of these neurons—an effect that outlasts $GABA_A$-receptor-mediated fast synaptic inhibition—and thus disinhibition of VP^{ChAT} neurons and the subsequent release of ACh into the BLA. This function of dynorphin is ultimately required for driving animals to pursue a reward that comes with an effort but is dispensable if the reward is obtainable at a low cost. On the other hand, through activation of KORs on NAc^{Pdyn} neurons, dynorphin induces autoinhibition of their projections to the VP, which fine-tunes the disinhibition of VP^{ChAT} neurons and the release of ACh into the BLA, thereby adjusting the intensity of an animal's actions to pursue reward. Our study thus uncovers that the $NAc^{Pdyn} \rightarrow VP^{GABA} \rightarrow VP^{ChAT}$ circuit has an important role in promoting reward-seeking behavior and also delineates its working mechanisms.

A notable observation, which is enabled by the newly developed dynorphin sensor,[39] is that dynorphin release from NAc^{Pdyn} neurons into the VP is triggered by a rewarding stimulus but not by an aversive one. This observation is at first glance surprising, as it is at odds with the prevailing notion that dynorphin/KOR conveys anti-reward signals. However, it is consistent with our further observation that dynorphin invigorates reward-seeking behaviors through the $VP^{ChAT} \rightarrow$ BLA cholinergic circuit and is also consistent with previous reports that Pdyn neurons[18–20] or dynorphin/KOR signaling[13–16] is involved in reward-seeking behaviors. The notion that dynorphin/KOR signaling is anti-reward is likely rooted in the specific brain areas examined and the methods used. For instance, infusion of KOR agonists into the NAc can result in the suppression of transmitter release from various inputs, including dopaminergic inputs and glutamatergic inputs that are critical for reward processing,[3,8] therefore causing aversive or dysphoric effects. Our study, on the other hand, probes the functions of dynorphin and KORs in the distinct elements of VP circuits, which are known to control motivational drive during reward-seeking behaviors.[27–32] Thus, the seemingly contradictory findings about dynorphin/KOR function can be explained by the divergent behavioral roles of neural circuits whereby this signaling system acts.

Neurons in subcortical nuclei, such as the NAc, the bed nucleus of the stria terminalis, the central amygdala, and hypothalamic areas, often express various neuropeptides that can be co-released with fast-acting neurotransmitters from the same neurons.[8,34,44,45] The development of CRISPR-Cas9 mutagenesis viruses has made it possible to study their functions in isolation.[46] The present study is in line with recent studies showing that neuropeptides have functions distinct from those of fast-acting neurotransmitters.[44,45] In our study, the effects of perturbing dynorphin/KOR signaling in the NAc → VP circuit on RTPP suggest that the slow-acting dynorphinergic transmission in this circuit is not essential for valence processing. Therefore, it will be interesting to further examine whether valence processing is dependent on fast-acting neurotransmitters in this circuit.

Previous studies indicate that glutamatergic neurons and GABAergic neurons in the VP play critical roles in valence-specific behaviors.[27,47–50] For example, it has been shown that the glutamatergic neurons are "negative-valence neurons (NVNs)" that mediate aversive response and punishment avoidance, whereas a subpopulation of VP GABAergic neurons are "positive-valence neurons (PVNs)" that mediate appetitive and reward-seeking behavior.[27] However, the GABAergic neurons are functionally heterogeneous. Apart from the PVNs, another subpopulation of VP GABAergic neurons show different encoding properties, being inhibited by salient stimuli irrespective of valence.[27] Therefore, it is believed that the complex interactions between the functionally distinct types of VP neurons orchestrate valence-specific behaviors, with the balance of activity between PVNs and NVNs determining reward seeking and punishment avoidance.[27,47–50]

In the present study, we show that activation of $NAc^{Pdyn} \rightarrow$ VP projections promotes reward-seeking behavior (Figures 3H–3K and S9) and also drives place preference (Figure S13). The former effect could be mediated by the disinhibition of VP cholinergic neurons, as discussed above. The latter effect, on the other hand, is likely mediated by a shift in balance between the PVNs and NVNs, which could be caused by an NAc^{Pdyn}-neuron-driven disinhibition of the PVNs and/or inhibition of the NVNs. We speculate that the above-mentioned subpopulation of GABAergic neurons, i.e., those that are inhibited by salient stimuli,[27] participate in the disinhibitory processes. Thus, during reward seeking or when $NAc^{Pdyn} \rightarrow$ VP projections are activated, these neurons are inhibited, disinhibiting PVNs and/or cholinergic neurons and thereby coordinating reward-approaching actions.

The cholinergic system has been implicated in multiple brain functions, including attention, learning, mood regulation, reward processing, and motivation.[28,30,37,43,51–56] In particular, cholinergic neurons in the VP and the NBM send dense projections to the BLA (Figure S5) that contribute to both fear learning and reward learning.[28,29,37,55–58] Therefore, the learning function of the $NAc^{Pdyn} \rightarrow$ VP circuit is likely mediated, at least in part, by VP and/or NBM cholinergic projections to the BLA. Interestingly, recent studies demonstrate that cholinergic projections to the

BLA promote reward responding (including licking) independent of learning and motor functions.[30,55] Our results are consistent with these findings and further reveal that these projections bidirectionally modulate the vigor of reward-seeking actions when the task is demanding. Of note, it has been shown that activation of NBM cholinergic projections to the BLA does not affect reward seeking in a PR task.[28] The difference between this result and ours likely reflects a functional distinction between the cholinergic neurons in the NBM and those in the VP.

Interestingly, it has been shown that BLA projections to the NAc drive reward-seeking behaviors.[59–61] Thus, a BLA→NAc^{Pdyn}→VP^{GABA}→VP^{ChAT}→BLA loop may exist and be critical for driving reward seeking. Alternatively, or in addition, projections from BLA Fezf2 neurons to the olfactory tubercle may also mediate the function of ACh in the BLA, as these projections have recently been shown to drive reward-seeking actions.[62] Future studies will delineate how ACh regulates distinct BLA circuits to influence reward-seeking actions as well as other functions. Moreover, future studies will also examine whether alterations in the NAc^{Pdyn}→VP^{GABA}→VP^{ChAT}→BLA circuit contribute to motivational disorders, including depression and drug addiction.

Limitations of the study

Previous studies have shown that cholinergic neurons in the basal forebrain can corelease ACh together with GABA or glutamate,[63,64] and VP cholinergic neurons projecting to the BLA may corelease ACh together with glutamate but not with GABA.[36] Thus, the disinhibition of cholinergic neurons by NAc^{Pdyn}→VP projections may cause corelease of ACh and glutamate in the BLA. The exact role of this corelease remains to be investigated. The NAc contains functionally distinct subregions, including shell and core. It has been shown that neurons in the lateral shell and medial shell differentially regulate dopamine neurons in the VTA.[65] Neurons in the ventral shell and dorsal shell also have different functions.[19] In this study we mainly focused on the NAc core region (Figures S6–S8). How other subregions regulate the VP needs further investigation. Finally, the VP expands considerably along the anteroposterior axis, with both the anterior and the posterior domains receiving NAc^{Pdyn} projections (Figure S2L). We examined dynorphin release in the posterior VP where the BLA-projecting cholinergic neurons are concentrated (Figure S5). Future studies will investigate the dynamics and functions of dynorphin in the anterior VP and determine how it might modulate the various types of neurons therein.

RESOURCE AVAILABILITY

Lead contact

Further information and requests for resources and reagents should be directed to and will be fulfilled by the lead contact, Qingtao Sun (qsun@cshl.edu).

Materials availability

This study did not generate new unique reagents.

Data and code availability

- The authors declare that the data supporting the findings of this study are available within the paper and its supplemental information files.
- All original code has been deposited at Figshare and is publicly available as of the date of publication.
- Any additional information required to reanalyze the data reported in this paper is available from the lead contact upon request.

ACKNOWLEDGMENTS

We thank Richard Palmiter for permission to use the *Pdyn*$^{flox/flox}$ mouse line; Karl Deisseroth for generously providing the AAV5-EF1α-fDIO-hChR2(H134R)-YFP virus; Radhashree Sharma, Charlotte Lee, and Darren Chen for technical assistance; and members of the Li laboratory for helpful discussions. This work was supported by grants from the National Institutes of Health (NIH) (R01MH108924, to B.L.) and the Cold Spring Harbor Laboratory and Northwell Health Affiliation (to B.L.).

AUTHOR CONTRIBUTIONS

Q.S., M.L., W.G., and B.L. designed research; Q.S. and M.L. performed research and analyzed data; W.G. made the initial observation that activation of Drd1 neurons in the NAc leads to robust acetylcholine release in the BLA; X.X. assisted with the PR task; C.D. and L.T. developed the dynorphin sensor; M.R.B. assisted with the *Pdyn*$^{flox/flox}$ mouse line; L.S.Z. developed the CRISPR-Cas9 system targeting *Oprk1*; Y.L. developed the acetylcholine sensor; and Q.S. and B.L. wrote the paper with inputs from all authors.

DECLARATION OF INTERESTS

The authors declare no competing interests.

STAR★METHODS

Detailed methods are provided in the online version of this paper and include the following:

- KEY RESOURCES TABLE
- EXPERIMENTAL MODEL AND STUDY PARTICIPANT DETAILS
- METHOD DETAILS
  - Viral vectors
  - Stereotaxic surgery and injection
  - Immunohistochemistry
  - Fluorescence *in situ* hybridization
  - *In vitro* electrophysiology
  - Measuring acetylcholine release in behaving mice
  - *In vivo* fiber photometry and data analysis
  - Go/no-go task
  - Testing the influence of the NAc^{Pdyn}→VP projections on licking behavior
  - Progressive ratio task
  - Real-time place aversion or preference test
  - Testing the influence of the NAc^{Pdyn}→VP projections on locomotion
  - Elevated plus maze test
  - Behavioral data acquisition and analysis
- QUANTIFICATION AND STATISTICAL ANALYSIS

SUPPLEMENTAL INFORMATION

Supplemental information can be found online at https://doi.org/10.1016/j.neuron.2025.03.018.

Received: October 2, 2024
Revised: February 7, 2025
Accepted: March 13, 2025
Published: April 15, 2025

REFERENCES

1. Chavkin, C. (2013). Dynorphin–still an extraordinarily potent opioid peptide. Mol. Pharmacol. *83*, 729–736. https://doi.org/10.1124/mol.112.083337.
2. Schwarzer, C. (2009). 30 years of dynorphins–new insights on their functions in neuropsychiatric diseases. Pharmacol. Ther. *123*, 353–370. https://doi.org/10.1016/j.pharmthera.2009.05.006.
3. Darcq, E., and Kieffer, B.L. (2018). Opioid receptors: drivers to addiction? Nat. Rev. Neurosci. *19*, 499–514. https://doi.org/10.1038/s41583-018-0028-x.
4. Tejeda, H.A., Wu, J., Kornspun, A.R., Pignatelli, M., Kashtelyan, V., Krashes, M.J., Lowell, B.B., Carlezon, W.A., Jr., and Bonci, A. (2017). Pathway- and Cell-Specific Kappa-Opioid Receptor Modulation of Excitation-Inhibition Balance Differentially Gates D1 and D2 Accumbens Neuron Activity. Neuron *93*, 147–163. https://doi.org/10.1016/j.neuron.2016.12.005.
5. Spanagel, R., Herz, A., and Shippenberg, T.S. (1992). Opposing tonically active endogenous opioid systems modulate the mesolimbic dopaminergic pathway. Proc. Natl. Acad. Sci. USA *89*, 2046–2050. https://doi.org/10.1073/pnas.89.6.2046.
6. Pomrenze, M.B., Cardozo Pinto, D.F., Neumann, P.A., Llorach, P., Tucciarone, J.M., Morishita, W., Eshel, N., Heifets, B.D., and Malenka, R.C. (2022). Modulation of 5-HT release by dynorphin mediates social deficits during opioid withdrawal. Neuron *110*, 4125–4143.e6. https://doi.org/10.1016/j.neuron.2022.09.024.
7. Ahrens, S., Wu, M.V., Furlan, A., Hwang, G.R., Paik, R., Li, H.H., Penzo, M.A., Tollkuhn, J., and Li, B. (2018). A Central Extended Amygdala Circuit That Modulates Anxiety. J. Neurosci. *38*, 5567–5583. https://doi.org/10.1523/JNEUROSCI.0705-18.2018.
8. Castro, D.C., and Bruchas, M.R. (2019). A Motivational and Neuropeptidergic Hub: Anatomical and Functional Diversity within the Nucleus Accumbens Shell. Neuron *102*, 529–552. https://doi.org/10.1016/j.neuron.2019.03.003.
9. Bruchas, M.R., Schindler, A.G., Shankar, H., Messinger, D.I., Miyatake, M., Land, B.B., Lemos, J.C., Hagan, C.E., Neumaier, J.F., Quintana, A., et al. (2011). Selective p38alpha MAPK deletion in serotonergic neurons produces stress resilience in models of depression and addiction. Neuron *71*, 498–511. https://doi.org/10.1016/j.neuron.2011.06.011.
10. Donahue, R.J., Landino, S.M., Golden, S.A., Carroll, F.I., Russo, S.J., and Carlezon, W.A., Jr. (2015). Effects of acute and chronic social defeat stress are differentially mediated by the dynorphin/kappa-opioid receptor system. Behav. Pharmacol. *26*, 654–663. https://doi.org/10.1097/FBP.0000000000000155.
11. Koob, G.F., Buck, C.L., Cohen, A., Edwards, S., Park, P.E., Schlosburg, J.E., Schmeichel, B., Vendruscolo, L.F., Wade, C.L., Whitfield, T.W., and George, O. (2014). Addiction as a stress surfeit disorder. Neuropharmacology *76*, 370–382. https://doi.org/10.1016/j.neuropharm.2013.05.024.
12. Koob, G.F., and Le Moal, M. (2008). Addiction and the brain antireward system. Annu. Rev. Psychol. *59*, 29–53. https://doi.org/10.1146/annurev.psych.59.103006.093548.
13. Cooper, S.J., Jackson, A., and Kirkham, T.C. (1985). Endorphins and food intake: kappa opioid receptor agonists and hyperphagia. Pharmacol. Biochem. Behav. *23*, 889–901. https://doi.org/10.1016/0091-3057(85)90088-7.
14. Morley, J.E., and Levine, A.S. (1983). Involvement of dynorphin and the kappa opioid receptor in feeding. Peptides *4*, 797–800. https://doi.org/10.1016/0196-9781(83)90069-4.
15. Sandoval-Caballero, C., Jara, J., Luarte, L., Jiménez, Y., Teske, J.A., and Perez-Leighton, C. (2024). Control of motivation for sucrose in the paraventricular hypothalamic nucleus by dynorphin peptides and the kappa opioid receptor. Appetite *200*, 107504. https://doi.org/10.1016/j.appet.2024.107504.
16. Sandoval-Caballero, C., Luarte, L., Jiménez, Y., Jaque, C., Cifuentes, F., Arenas, G.A., Figueroa, M., Jara, J., Olszewski, P.K., Teske, J.A., and Perez-Leighton, C.E. (2023). Meta-analysis of pre-clinical studies on the effects of opioid receptor ligands on food intake, motivation, and choice. Neurosci. Biobehav. Rev. *152*, 105288. https://doi.org/10.1016/j.neubiorev.2023.105288.
17. Cayir, S., Zhornitsky, S., Barzegary, A., Sotomayor-Carreño, E., Sarfo-Ansah, W., Funaro, M.C., Matuskey, D., and Angarita, G. (2024). A review of the kappa opioid receptor system in opioid use. Neurosci. Biobehav. Rev. *162*, 105713. https://doi.org/10.1016/j.neubiorev.2024.105713.
18. Xiao, X., Deng, H., Furlan, A., Yang, T., Zhang, X., Hwang, G.R., Tucciarone, J., Wu, P., He, M., Palaniswamy, R., et al. (2020). A Genetically Defined Compartmentalized Striatal Direct Pathway for Negative Reinforcement. Cell *183*, 211–227.e20. https://doi.org/10.1016/j.cell.2020.08.032.
19. Al-Hasani, R., McCall, J.G., Shin, G., Gomez, A.M., Schmitz, G.P., Bernardi, J.M., Pyo, C.O., Park, S.I., Marcinkiewcz, C.M., Crowley, N.A., et al. (2015). Distinct Subpopulations of Nucleus Accumbens Dynorphin Neurons Drive Aversion and Reward. Neuron *87*, 1063–1077. https://doi.org/10.1016/j.neuron.2015.08.019.
20. Ibrahim, K.M., Massaly, N., Yoon, H.J., Sandoval, R., Widman, A.J., Heuermann, R.J., Williams, S., Post, W., Pathiranage, S., Lintz, T., et al. (2024). Dorsal hippocampus to nucleus accumbens projections drive reinforcement via activation of accumbal dynorphin neurons. Nat. Commun. *15*, 750. https://doi.org/10.1038/s41467-024-44836-9.
21. Bals-Kubik, R., Ableitner, A., Herz, A., and Shippenberg, T.S. (1993). Neuroanatomical sites mediating the motivational effects of opioids as mapped by the conditioned place preference paradigm in rats. J. Pharmacol. Exp. Ther. *264*, 489–495. https://doi.org/10.1016/S0022-3565(25)10296-6.
22. Heimer, L., Harlan, R.E., Alheid, G.F., Garcia, M.M., and de Olmos, J. (1997). Substantia innominata: a notion which impedes clinical-anatomical correlations in neuropsychiatric disorders. Neuroscience *76*, 957–1006. https://doi.org/10.1016/s0306-4522(96)00405-8.
23. Humphries, M.D., and Prescott, T.J. (2010). The ventral basal ganglia, a selection mechanism at the crossroads of space, strategy, and reward. Prog. Neurobiol. *90*, 385–417. https://doi.org/10.1016/j.pneurobio.2009.11.003.
24. Root, D.H., Melendez, R.I., Zaborszky, L., and Napier, T.C. (2015). The ventral pallidum: Subregion-specific functional anatomy and roles in motivated behaviors. Prog. Neurobiol. *130*, 29–70. https://doi.org/10.1016/j.pneurobio.2015.03.005.
25. Smith, K.S., Tindell, A.J., Aldridge, J.W., and Berridge, K.C. (2009). Ventral pallidum roles in reward and motivation. Behav. Brain Res. *196*, 155–167. https://doi.org/10.1016/j.bbr.2008.09.038.
26. Wulff, A.B., Tooley, J., Marconi, L.J., and Creed, M.C. (2019). Ventral pallidal modulation of aversion processing. Brain Res. *1713*, 62–69. https://doi.org/10.1016/j.brainres.2018.10.010.
27. Stephenson-Jones, M., Bravo-Rivera, C., Ahrens, S., Furlan, A., Xiao, X., Fernandes-Henriques, C., and Li, B. (2020). Opposing Contributions of GABAergic and Glutamatergic Ventral Pallidal Neurons to Motivational Behaviors. Neuron *105*, 921–933.e5. https://doi.org/10.1016/j.neuron.2019.12.006.
28. Crouse, R.B., Kim, K., Batchelor, H.M., Girardi, E.M., Kamaletdinova, R., Chan, J., Rajebhosale, P., Pittenger, S.T., Role, L.W., Talmage, D.A., et al. (2020). Acetylcholine is released in the basolateral amygdala in response to predictors of reward and enhances the learning of cue-reward contingency. eLife *9*, e57335. https://doi.org/10.7554/eLife.57335.
29. Aitta-aho, T., Hay, Y.A., Phillips, B.U., Saksida, L.M., Bussey, T.J., Paulsen, O., and Apergis-Schoute, J. (2018). Basal Forebrain and Brainstem Cholinergic Neurons Differentially Impact Amygdala Circuits and Learning-Related Behavior. Curr. Biol. *28*, 2557–2569.e4. https://doi.org/10.1016/j.cub.2018.06.064.

30. Kimchi, E.Y., Burgos-Robles, A., Matthews, G.A., Chakoma, T., Patarino, M., Weddington, J.C., Siciliano, C., Yang, W., Foutch, S., Simons, R., et al. (2024). Reward contingency gates selective cholinergic suppression of amygdala neurons. eLife *12*, RP89093. https://doi.org/10.7554/eLife.89093.

31. Ottenheimer, D.J., Bari, B.A., Sutlief, E., Fraser, K.M., Kim, T.H., Richard, J.M., Cohen, J.Y., and Janak, P.H. (2020). A quantitative reward prediction error signal in the ventral pallidum. Nat. Neurosci. *23*, 1267–1276. https://doi.org/10.1038/s41593-020-0688-5.

32. Richard, J.M., Ambroggi, F., Janak, P.H., and Fields, H.L. (2016). Ventral Pallidum Neurons Encode Incentive Value and Promote Cue-Elicited Instrumental Actions. Neuron *90*, 1165–1173. https://doi.org/10.1016/j.neuron.2016.04.037.

33. Tuna, T., Banks, T., Glickert, G., Sevinc, C., Nair, S.S., and Unal, G. (2025). Basal forebrain innervation of the amygdala: an anatomical and computational exploration. Brain Struct. Funct. *230*, 30. https://doi.org/10.1007/s00429-024-02886-1.

34. Fellinger, L., Jo, Y.S., Hunker, A.C., Soden, M.E., Elum, J., Juarez, B., and Zweifel, L.S. (2021). A midbrain dynorphin circuit promotes threat generalization. Curr. Biol. *31*, 4388–4396.e5. https://doi.org/10.1016/j.cub.2021.07.047.

35. Jing, M., Li, Y., Zeng, J., Huang, P., Skirzewski, M., Kljakic, O., Peng, W., Qian, T., Tan, K., Zou, J., et al. (2020). An optimized acetylcholine sensor for monitoring in vivo cholinergic activity. Nat. Methods *17*, 1139–1146. https://doi.org/10.1038/s41592-020-0953-2.

36. Barabás, B., Reéb, Z., Papp, O.I., and Hájos, N. (2024). Functionally linked amygdala and prefrontal cortical regions are innervated by both single and double projecting cholinergic neurons. Front. Cell. Neurosci. *18*, 1426153. https://doi.org/10.3389/fncel.2024.1426153.

37. Jiang, L., Kundu, S., Lederman, J.D., López-Hernández, G.Y., Ballinger, E.C., Wang, S., Talmage, D.A., and Role, L.W. (2016). Cholinergic Signaling Controls Conditioned Fear Behaviors and Enhances Plasticity of Cortical-Amygdala Circuits. Neuron *90*, 1057–1070. https://doi.org/10.1016/j.neuron.2016.04.028.

38. Copits, B.A., Gowrishankar, R., O'Neill, P.R., Li, J.N., Girven, K.S., Yoo, J.J., Meshik, X., Parker, K.E., Spangler, S.M., Elerding, A.J., et al. (2021). A photoswitchable GPCR-based opsin for presynaptic inhibition. Neuron *109*, 1791–1809.e11. https://doi.org/10.1016/j.neuron.2021.04.026.

39. Dong, C., Gowrishankar, R., Jin, Y., He, X.J., Gupta, A., Wang, H., Sayar-Atasoy, N., Flores, R.J., Mahe, K., Tjahjono, N., et al. (2024). Unlocking opioid neuropeptide dynamics with genetically encoded biosensors. Nat. Neurosci. *27*, 1844–1857. https://doi.org/10.1038/s41593-024-01697-1.

40. Bloodgood, D.W., Hardaway, J.A., Stanhope, C.M., Pati, D., Pina, M.M., Neira, S., Desai, S., Boyt, K.M., Palmiter, R.D., and Kash, T.L. (2021). Kappa opioid receptor and dynorphin signaling in the central amygdala regulates alcohol intake. Mol. Psychiatry *26*, 2187–2199. https://doi.org/10.1038/s41380-020-0690-z.

41. Chavkin, C., Cohen, J.H., and Land, B.B. (2019). Repeated Administration of Norbinaltorphimine Produces Cumulative Kappa Opioid Receptor Inactivation. Front. Pharmacol. *10*, 88. https://doi.org/10.3389/fphar.2019.00088.

42. Deng, H., Xiao, X., Yang, T., Ritola, K., Hantman, A., Li, Y., Huang, Z.J., and Li, B. (2021). A genetically defined insula-brainstem circuit selectively controls motivational vigor. Cell *184*, 6344–6360.e18. https://doi.org/10.1016/j.cell.2021.11.019.

43. Picciotto, M.R., Higley, M.J., and Mineur, Y.S. (2012). Acetylcholine as a neuromodulator: cholinergic signaling shapes nervous system function and behavior. Neuron *76*, 116–129. https://doi.org/10.1016/j.neuron.2012.08.036.

44. Soden, M.E., Yee, J.X., and Zweifel, L.S. (2023). Circuit coordination of opposing neuropeptide and neurotransmitter signals. Nature *619*, 332–337. https://doi.org/10.1038/s41586-023-06246-7.

45. Li, H., Namburi, P., Olson, J.M., Borio, M., Lemieux, M.E., Beyeler, A., Calhoon, G.G., Hitora-Imamura, N., Coley, A.A., Libster, A., et al. (2022). Neurotensin orchestrates valence assignment in the amygdala. Nature *608*, 586–592. https://doi.org/10.1038/s41586-022-04964-y.

46. Hunker, A.C., Soden, M.E., Krayushkina, D., Heymann, G., Awatramani, R., and Zweifel, L.S. (2020). Conditional Single Vector CRISPR/SaCas9 Viruses for Efficient Mutagenesis in the Adult Mouse Nervous System. Cell Rep. *30*, 4303–4316.e6. https://doi.org/10.1016/j.celrep.2020.02.092.

47. Faget, L., Oriol, L., Lee, W.C., Zell, V., Sargent, C., Flores, A., Hollon, N.G., Ramanathan, D., and Hnasko, T.S. (2024). Ventral pallidum GABA and glutamate neurons drive approach and avoidance through distinct modulation of VTA cell types. Nat. Commun. *15*, 4233. https://doi.org/10.1038/s41467-024-48340-y.

48. Shuvaev, S.A., Tran, N.B., Stephenson-Jones, M., Li, B., and Koulakov, A.A. (2020). Neural Networks With Motivation. Front. Syst. Neurosci. *14*, 609316. https://doi.org/10.3389/fnsys.2020.609316.

49. Zhu, C., Yao, Y., Xiong, Y., Cheng, M., Chen, J., Zhao, R., Liao, F., Shi, R., and Song, S. (2017). Somatostatin Neurons in the Basal Forebrain Promote High-Calorie Food Intake. Cell Rep. *20*, 112–123. https://doi.org/10.1016/j.celrep.2017.06.007.

50. Heinsbroek, J.A., Bobadilla, A.C., Dereschewitz, E., Assali, A., Chalhoub, R.M., Cowan, C.W., and Kalivas, P.W. (2020). Opposing Regulation of Cocaine Seeking by Glutamate and GABA Neurons in the Ventral Pallidum. Cell Rep. *30*, 2018–2027.e3. https://doi.org/10.1016/j.celrep.2020.01.023.

51. Mineur, Y.S., and Picciotto, M.R. (2021). The role of acetylcholine in negative encoding bias: Too much of a good thing? Eur. J. Neurosci. *53*, 114–125. https://doi.org/10.1111/ejn.14641.

52. Mineur, Y.S., and Picciotto, M.R. (2023). How can I measure brain acetylcholine levels in vivo? Advantages and caveats of commonly used approaches. J. Neurochem. *167*, 3–15. https://doi.org/10.1111/jnc.15943.

53. Collins, A.L., Aitken, T.J., Greenfield, V.Y., Ostlund, S.B., and Wassum, K.M. (2016). Nucleus Accumbens Acetylcholine Receptors Modulate Dopamine and Motivation. Neuropsychopharmacology *41*, 2830–2838. https://doi.org/10.1038/npp.2016.81.

54. Nunes, E.J., Kebede, N., Bagdas, D., and Addy, N.A. (2022). Cholinergic and dopaminergic-mediated motivated behavior in healthy states and in substance use and mood disorders. J. Exp. Anal. Behav. *117*, 404–419. https://doi.org/10.1002/jeab.747.

55. Kim, R., Ananth, M.R., Desai, N.S., Role, L.W., and Talmage, D.A. (2024). Distinct subpopulations of ventral pallidal cholinergic projection neurons encode valence of olfactory stimuli. Cell Rep. *43*, 114009. https://doi.org/10.1016/j.celrep.2024.114009.

56. Ji, Y.W., Shen, Z.L., Zhang, X., Zhang, K., Jia, T., Xu, X., Geng, H., Han, Y., Yin, C., Yang, J.J., et al. (2023). Plasticity in ventral pallidal cholinergic neuron-derived circuits contributes to comorbid chronic pain-like and depression-like behaviour in male mice. Nat. Commun. *14*, 2182. https://doi.org/10.1038/s41467-023-37968-x.

57. Woolf, N.J. (1991). Cholinergic systems in mammalian brain and spinal cord. Prog. Neurobiol. *37*, 475–524. https://doi.org/10.1016/0301-0082(91)90006-m.

58. Zaborszky, L., van den Pol, A., and Gyengesi, E. (2012). The basal forebrain cholinergic projection system in mice. In The Mouse Nervous System (Elsevier), pp. 684–718. https://doi.org/10.1016/B978-0-12-369497-3.10028-7.

59. Stuber, G.D., Sparta, D.R., Stamatakis, A.M., van Leeuwen, W.A., Hardjoprajitno, J.E., Cho, S., Tye, K.M., Kempadoo, K.A., Zhang, F., Deisseroth, K., and Bonci, A. (2011). Excitatory transmission from the amygdala to nucleus accumbens facilitates reward seeking. Nature *475*, 377–380. https://doi.org/10.1038/nature10194.

60. Britt, J.P., Benaliouad, F., McDevitt, R.A., Stuber, G.D., Wise, R.A., and Bonci, A. (2012). Synaptic and behavioral profile of multiple glutamatergic

inputs to the nucleus accumbens. Neuron *76*, 790–803. https://doi.org/10.1016/j.neuron.2012.09.040.

61. Namburi, P., Beyeler, A., Yorozu, S., Calhoon, G.G., Halbert, S.A., Wichmann, R., Holden, S.S., Mertens, K.L., Anahtar, M., Felix-Ortiz, A.C., et al. (2015). A circuit mechanism for differentiating positive and negative associations. Nature *520*, 675–678. https://doi.org/10.1038/nature14366.
62. Zhang, X., Guan, W., Yang, T., Furlan, A., Xiao, X., Yu, K., An, X., Galbavy, W., Ramakrishnan, C., Deisseroth, K., et al. (2021). Genetically identified amygdala-striatal circuits for valence-specific behaviors. Nat. Neurosci. *24*, 1586–1600. https://doi.org/10.1038/s41593-021-00927-0.
63. Saunders, A., Granger, A.J., and Sabatini, B.L. (2015). Corelease of acetylcholine and GABA from cholinergic forebrain neurons. eLife *4*, e06412. https://doi.org/10.7554/eLife.06412.
64. Sun, Q., Li, X., Ren, M., Zhao, M., Zhong, Q., Ren, Y., Luo, P., Ni, H., Zhang, X., Zhang, C., et al. (2019). A whole-brain map of long-range inputs to GABAergic interneurons in the mouse medial prefrontal cortex. Nat. Neurosci. *22*, 1357–1370. https://doi.org/10.1038/s41593-019-0429-9.
65. Yang, H., de Jong, J.W., Tak, Y., Peck, J., Bateup, H.S., and Lammel, S. (2018). Nucleus Accumbens Subnuclei Regulate Motivated Behavior via Direct Inhibition and Disinhibition of VTA Dopamine Subpopulations. Neuron *97*, 434–449.e4. https://doi.org/10.1016/j.neuron.2017.12.022.
66. Schneeberger, M., Parolari, L., Das Banerjee, T., Bhave, V., Wang, P., Patel, B., Topilko, T., Wu, Z., Choi, C.H.J., Yu, X., et al. (2019). Regulation of Energy Expenditure by Brainstem GABA Neurons. Cell *178*, 672–685.e12. https://doi.org/10.1016/j.cell.2019.05.048.
67. Taniguchi, H., He, M., Wu, P., Kim, S., Paik, R., Sugino, K., Kvitsiani, D., Fu, Y., Lu, J., Lin, Y., et al. (2011). A resource of Cre driver lines for genetic targeting of GABAergic neurons in cerebral cortex. Neuron *71*, 995–1013. https://doi.org/10.1016/j.neuron.2011.07.026.
68. Yang, T., Yu, K., Zhang, X., Xiao, X., Chen, X., Fu, Y., and Li, B. (2023). Plastic and stimulus-specific coding of salient events in the central amygdala. Nature *616*, 510–519. https://doi.org/10.1038/s41586-023-05910-2.
69. Li, H., Penzo, M.A., Taniguchi, H., Kopec, C.D., Huang, Z.J., and Li, B. (2013). Experience-dependent modification of a central amygdala fear circuit. Nat. Neurosci. *16*, 332–339. https://doi.org/10.1038/nn.3322.
70. Hodos, W. (1961). Progressive ratio as a measure of reward strength. Science *134*, 943–944. https://doi.org/10.1126/science.134.3483.943.
71. Richardson, N.R., and Roberts, D.C. (1996). Progressive ratio schedules in drug self-administration studies in rats: a method to evaluate reinforcing efficacy. J. Neurosci. Methods *66*, 1–11. https://doi.org/10.1016/0165-0270(95)00153-0.

STAR★METHODS

KEY RESOURCES TABLE

REAGENT or RESOURCE	SOURCE	IDENTIFIER
Antibodies		
Chicken anti-GFP	AvesLabs	Cat#: GFP1020; RRID:AB_10000240
Rabbit anti-RFP	Rockland	Cat#: 600-401-379; RRID:AB_2209751
Goat anti- choline acetyltransferase (ChAT)	Sigma-Aldrich	Cat#: AB144P; RRID: AB_2079751
Bacterial and virus strains		
AAV-EF1a-DIO-hChR2(H134R)-EYFP-WPRE-HGHpA	Gift from Karl Deisseroth (unpublished)	(Addgene viral prep # 20298-AAV5; http://n2t.net/addgene:20298; RRID:Addgene_20298)
AAV-hSyn-DIO-mCherry	Gift from Bryan Roth (unpublished)	Addgene viral prep # 50459-AAV2; http://n2t.net/addgene:50459; RRID:Addgene_50459
AAV-EF1a-fDIO-mCherry	Gift from Karl Deisseroth (unpublished)	Addgene viral prep # 114471-AAV5; http://n2t.net/addgene:114471; RRID:Addgene_114471
AAV-hSyn-mCherry	Gift from Karl Deisseroth (unpublished)	Addgene viral prep # 114472-AAV8; http://n2t.net/addgene:114472; RRID:Addgene_114472
AAV-Ef1a-DIO-PPO-mVenus	Copits et al.[38]	Addgene viral prep # 139505-AAV9; http://n2t.net/addgene:139505; RRID:Addgene_139505
AAV-EF1a-fDIO-Cre	Schneeberger et al.[66]	Addgene viral prep # 121675-AAV8; http://n2t.net/addgene:121675; RRID:Addgene_121675
AAV9/CAG-FLEX-ArchT-GFP	University of North Carolina vector core facility (Chapel Hill, North Carolina, USA)	N/A
AAV8-hSyn-mCherry-Cre	University of North Carolina vector core facility (Chapel Hill, North Carolina, USA)	N/A
AAV-hSyn-gACh3.0	WZ Biosciences	N/A
AAV-hSyn-gACh3.0-mut	WZ Biosciences	N/A
AAV-hSyn-klight1.3	Lin Tian lab	N/A
AAV1-Flex-SaCas9-sgOprk1	Larry Zweifel lab	N/A
AAV1-Flex-SaCas9-U6-sg-Rosa26	Larry Zweifel lab	N/A
AAV1-Flex-eGFP-Kash	Larry Zweifel lab	N/A
AAV5-EF1α-fDIO-hChR2(H134R)-YFP	Karl Deisseroth lab	N/A
AAV9-CAGGS-Flex-mKate-T2A-TVA	HHMI Janelia Research Campus	N/A
AAV9-CAGGS-Flex-mKate-T2A-N2c-G	HHMI Janelia Research Campus	N/A
Rbv-CVS-N2c-dG-GFP	HHMI Janelia Research Campus	N/A
AAV-DIO-EGFP-2A-TK	BrainVTA	Cat#: PT-0087
HSV-dTK-hUbc-tdTomato	BrainVTA	Cat#: H03001
Chemicals, peptides, and recombinant proteins		
Alexa Fluor555 Conjugate Cholera Toxin Subunit B	Thermo Fisher	Cat# C22843
norBNI	Sigma-Aldrich	Cat# 5.08017
Critical commercial assays		
RNAscope Probe against *Pdyn*	ACD Bio	Cat#: 318771-C2
RNAscope Probe against *mCherry*	ACD Bio	Cat#: 431201-C3
RNAscope Probe against *GFP*	ACD Bio	Cat#: 400281-C2

(*Continued on next page*)

Continued

REAGENT or RESOURCE	SOURCE	IDENTIFIER
RNAscope Probe against *Oprk1*	ACD Bio	Cat#: 316111-C1
RNAscope Probe against *Gad2*	ACD Bio	Cat#: 439371-C2 and C3
RNAscope Probe against *Tshz1*	ACD Bio	Cat#: 494291-C3
RNAscope Probe against *Drd1*	ACD Bio	Cat#: 406491-C1
RNAscope Probe against *Drd2*	ACD Bio	Cat#: 406501-C3
RNAscope Probe against *Slc17a6*	ACD Bio	Cat#: 319171-C3
RNAscope Probe against *tdTomato*	ACD Bio	Cat#: 317041-C1
RNAscope Probe against *ChAT*	ACD Bio	Cat#: 410071-C3
Experimental models: Organisms/strains		
Mouse: Pdyn-Cre (B6;129S-Pdyntm1.1(cre)Mjkr/LowlJ)	The Jackson Laboratory	Strain #:027958
Mouse: Gad2-Cre (STOCK Gad2tm2(cre)Zjh/J)	The Jackson Laboratory	Strain #:010802
Mouse: ChAT-Cre- Δneo (B6.129S-Chattm1(cre)Lowl/MwarJ)	The Jackson Laboratory	Strain #: 031661
Mouse: ChAT-Flpo (B6.Cg-Chattm1.1(flpo) Rmcld/J)	The Jackson Laboratory	Strain #:036281
Mouse: Vgat-Cre (B6J.129S6(FVB)-Slc32a1tm2(cre)Lowl/MwarJ)	The Jackson Laboratory	Strain #:028862
Mouse: C57BL/6J	The Jackson Laboratory	Strain #: 000664
Mouse: Adora2a-Cre (B6.FVB(Cg)-Tg(Adora2a-cre) KG139Gsat/Mmucd)	MMRRC	RRID: MMRRC_036158-UCD
Mouse: Pdyn-flox/flox	Richard Palmiter lab	N/A
Mouse: Tshz1-Cre	This paper	N/A
Software and algorithms		
ImageJ (Fiji) software	NIH	https://fiji.sc/
MATLAB	Mathworks	https://www.mathworks.com/products/matlab.html
GraphPad Prism 7	GraphPad Software	https://www.graphpad.com/
Clampfit	Molecular Devices	https://www.moleculardevices.com/products/axon-patch-clamp-system/acquisition-and-analysis-software/pclamp-software-suite
Original code	This paper	https://figshare.com/articles/software/Matlab_codes_for_Pdyn_paper/28735139

EXPERIMENTAL MODEL AND STUDY PARTICIPANT DETAILS

Male and female mice (2–4 months old) were used for all the experiments. Mice were housed under a 12-h light/12-h dark cycle (light from 7 a.m. to 7 p.m.) with a constant room temperature of 21 °C and 65% humidity. Mice were housed in groups of 2–5. Food and water were available ad libitum before the start of experiments. All experiments were performed during the light cycle. Littermates were randomly assigned to different groups before the experiments. All experimental procedures were approved by the Institutional Animal Care and Use Committee of Cold Spring Harbor Laboratory and performed in accordance with the US National Institutes of Health guidelines.

The *Tshz1*^{Cre} knockin mouse driver line, in which the expression of Cre recombinase is driven by the endogenous *Tshz1* promoter, was generated as previously described.[18] A gene-targeting vector for *Tshz1*^{Cre} was generated using a PCR-based cloning approach[67] to insert a *2A-Cre* construct immediately before the STOP codon of the *Tshz1* gene. The targeting vector was linearized and transfected into a 129SVj/B6 F1 hybrid ES cell line (V6.5, Open Biosystems). G418-resistant ES clones were first screened by PCR and then confirmed by Southern blotting using probes against the 5′ and 3′ homology arms of the targeted site.

PdynCre (Strain #:027958), Gad2Cre (Strain #:010802), ChatCre (Strain #:031661), ChatFlpO (Strain #:036281), VgatCre (Strain #:028862), and C57BL/6J (Strain #:000664) mice were purchased from the Jackson Laboratory. *Adora2a-Cre* mice (RRID: MMRRC_036158-UCD) were purchased from MMRRC. The *Pdyn*$^{flox/flox}$ mouse line was described previously.[40]

METHOD DETAILS

Viral vectors

AAV-EF1a-DIO-hChR2(H134R)-EYFP-WPRE-HGHpA (AAV5, 1.38×10^{13} genome copies (GC) per ml), AAV-hSyn-DIO-mCherry (AAV2, 2×10^{13} GC per ml), AAV-EF1a-fDIO-mCherry (AAV5, 2.3×10^{13} GC per ml), AAV-hSyn-mCherry (AAV8, 2.6×10^{13} GC per ml), AAV-Ef1a-DIO-PPO-mVenus (AAV9, 1×10^{13} GC per ml), AAV-EF1a-fDIO-Cre (AAV8, 1×10^{13} GC per ml) were purchased from Addgene. rAAV9/CAG-FLEX-ArchT-GFP (4.7×10^{12} GC per ml), AAV8-hSyn-mCherry-Cre (5×10^{12} GC per ml) were purchased from University of North Carolina Vector Core Facility. AAV-hSyn-gACh3.0 (1.3×10^{13} GC per ml) and AAV-hSyn-gACh3.0-mut (1.3×10^{13} GC per ml) were purchased from WZ bio. AAV-hSyn-klight1.3 was generated by Lin Tian lab. AAV1-Flex-SaCas9-sgOprk1, AAV1-Flex-SaCas9-U6-sg-Rosa26 and AAV1-Flex-eGFP-Kash was generated by Larry Zweifel lab. AAV5-EF1α-fDIO-hChR2(H134R)-YFP (5×10^{12} GC per ml) was generated by Deisseroth lab. AAV9-CAGGS-Flex-mKate-T2A-TVA (5×10^{12} GC per ml), AAV9-CAGGS-Flex-mKate-T2A-N2c-G (5×10^{12} GC per ml) and Rbv-CVS-N2c-dG-GFP (5×10^{8} plaque-forming units (PFUs) per ml) were generated by HHMI Janelia Research Campus. AAV-DIO-EGFP-2A-TK (2.66×10^{12} GC per ml) and HSV-dTK-hUbc-tdTomato (1.0×10^{9} PFUs per ml) were purchased from BrainVTA. All viral vectors were aliquoted and stored at -80 °C until use.

Stereotaxic surgery and injection

All surgeries were performed under aseptic conditions, and body temperature was maintained with a heating pad. Standard surgical procedures were used for stereotaxic injection and implantation, as previously described.[18,62,68] Briefly, mice were anesthetized with isoflurane (2% at the beginning for induction and 1%–1.5% for the rest of the surgery) and positioned in a stereotaxic frame. The frame was linked to a digital mouse brain atlas to guide the targeting of different brain structures (Angle Two Stereotaxic System, Leica Biosystems Division of Leica). The following stereotaxic coordinates in anteroposterior axis (AP), mediolateral axis (ML), and dorsoventral axis (DV) (all in mm in reference to Bregma) were used for the NAc: AP 1.1, ML 1.2, and DV -4.8; for the VP: AP 0, ML 1.5, and DV -5; for the BLA: AP -1.65, ML 3.3, and DV -4.8; and for the VMH: AP -1.6, ML 0.35, and DV -5.5. 200 – 300 nl of viral solution was injected at a speed of 1-2 nl/s. For AAVs, we typically waited at least 3-4 weeks after the injection to allow viral expression. For RV tracing, we injected the TVA and G helper viruses (at a ratio of 1:2 (volume:volume), 150 nl in total) first, and injected the RV (300 nl) 2-3 weeks later. We waited for 7 days after RV injection before collecting the brains for histological analysis. For HSV tracing, we injected the helper virus (150 – 200 nl) first, and injected the HSV (200 nl) 3 weeks later. We waited for 5 days after HSV injection before collecting the brains for histological analysis.

To examine the functional projections from the NAc to VP neurons and the disinhibition effects, AAV-EF1a-DIO-hChR2(H134R)-EYFP-WPRE-HGHpA was bilaterally injected into the NAc of *Pdyn*^{Cre};*ChAT*^{FlpO} mice (7-8 weeks old) in a volume of 300 nl for each site, and AAV-EF1a-fDIO-mCherry was bilaterally injected into the VP of the same mice in a volume of 300 nl for each side. These mice were subjected to slice electrophysiology experiments 2-3 weeks later. To check the disinhibition of cholinergic neurons in vivo, 300 nl AAV-EF1a-DIO-hChR2(H134R)-EYFP-WPRE-HGHpA was bilaterally injected into the NAc of *Pdyn*^{Cre} mice. A mixture of AAV-hSyn-mCherry and AAV-hSyn-gACh3.0 (1:10, volume:volume), or AAV-hSyn-mCherry and AAV-hSyn-gACh3.0-mut (1:10 in volume), was injected into the BLA of the same mice. For the optogenetic activation, 300 nl of AAV-EF1a-DIO-hChR2(H134R)-EYFP-WPRE-HGHpA was bilaterally injected into the NAc of *Tshz1*^{Cre} or *Adora2a-Cre* mice, and a mixture of AAV-hSyn-mCherry and AAV-hSyn-gACh3.0 (1:10, volume:volume) was injected into the BLA. For the activation of Pdyn^{+} terminals from the hypothalamus, 300 nl of AAV-EF1a-DIO-hChR2(H134R)-EYFP-WPRE-HGHpA was bilaterally injected into the VMH of *Pdyn*^{Cre} animals, and a mixture of AAV-hSyn-mCherry and AAV-hSyn-gACh3.0 (1:10, volume:volume) was injected into the BLA. For optogenetic inhibition, 300 nl of AAV-Ef1a-DIO-PPO-Venus was bidirectionally injected into the NAc, and a mixture of AAV-hSyn-mCherry and AAV-hSyn-gACh3.0 (1:10, volume:volume) was injected into the BLA.

For measuring the dynorphin sensor klight1.3 with fiber photometry, 300 nl of AAV8-hSyn-mCherry-Cre was bidirectionally injected into the NAc of *Pdyn*$^{flox/flox}$ animals or wild-type (WT) control animals. 300 nl of AAV-hSyn-klight1.3 was injected into the VP. After 4 weeks of virus expression, the animals were used for fiber photometry. To measure acetylcholine release in the BLA in response to photo-simulation of NAc neurons with or without *Pdyn* expression in the NAc, a mixture of AAV8-hSyn-mCherry-Cre and AAV-EF1a-DIO-hChR2(H134R)-EYFP-WPRE-HGHpA (1:1, volume:volume) was injected into the NAc, and a mixture of AAV-hSyn-mCherry and AAV-hSyn-gACh3.0 (1:10, volume:volume) was injected into the BLA. After 4 weeks of virus expression, the animals were used for fiber photometry.

To test the role of KORs in GABAergic neurons in the VP, AAV1-Flex-SaCas9-sgOprk1 or AAV1-Flex-SaCas9-U6-sg-Rosa26 was bidirectionally injected into the VP of *GAD2*^{Cre} mice, and a mixture of AAV-hSyn-mCherry and AAV-hSyn-gACh3.0 (1:10, volume:volume) was injected into the BLA. After 4 weeks of virus expression, the animals were used for fiber photometry. For the RTPP test in mice in which the expression of KORs was knocked down in GABAergic neurons in the VP, AAV1-Flex-SaCas9-sgOprk1 or AAV1-Flex-SaCas9-U6-sg-Rosa26 was bidirectionally injected into the VP, and 300 nl of AAV-EF1a-DIO-hChR2(H134R)-EYFP-WPRE-HGHpA was bilaterally injected into the NAc of of *GAD2*^{Cre} mice. To determine the role of KORs on VP GABAergic neurons in disinhibiting VP cholinergic neurons, AAV-EF1a-DIO-hChR2(H134R)-EYFP-WPRE-HGHpA was bilaterally injected into the NAc of *Gad2*^{Cre};*ChAT*^{FlpO} mice (7-8 weeks old) in a volume of 300 nl for each site, and a mixture of AAV-EF1a-fDIO-mCherry and

AAV1-Flex-SaCas9-sgOprk1 (or AAV1-Flex-SaCas9-U6-sg-Rosa26) was bilaterally injected into the VP in a volume of 300 nl for each side (1:1, volume:volume). These mice were subjected to slice electrophysiology experiments 2-3 weeks later.

To test the role of KORs in NAc^{Pdyn} neurons, a mixture of AAV-EF1a-DIO-hChR2(H134R)-EYFP-WPRE-HGHpA and AAV1-Flex-SaCas9-sgOprk1 (or AAV1-Flex-SaCas9-U6-sg-Rosa26) was bilaterally injected into the NAc of $Pdyn^{Cre}$ mice in a volume of 300 nl for each side (1:1, volume:volume). A mixture of AAV-hSyn-mCherry and AAV-hSyn-gACh3.0 (1:10, volume:volume) was injected into the BLA for fiber photometry. For electrophysiology recording in acute slices, a mixture of AAV-EF1a-DIO-hChR2(H134R)-EYFP-WPRE-HGHpA and AAV1-Flex-SaCas9-sgOprk1 (or AAV1-Flex-SaCas9-U6-sgRosa26) was injected into the NAc $Pdyn^{Cre}$;$ChAT^{FlpO}$ mice in a volume of 300 nl (1:1, volume:volume). 300 nl of AAV-EF1a-fDIO-mCherry was injected into the VP of the same mice to label cholinergic neurons.

For photo-activation of cholinergic terminals in the BLA, AAV5-EF1α-fDIO-hChR2(H134R)-YFP was bilaterally injected into the VP of $ChAT^{Flpo}$ mice in a volume of 300 nl for each side. For photo-inhibition of cholinergic terminals in the BLA, a mixture of AAV-Ef1a-DIO-PPO-Venus and AAV-EF1a-fDIO-Cre was bilaterally injected into the VP of $ChAT^{Flpo}$ mice in a volume of 300 nl for each side (1:1, volume:volume).

For *in vivo* optogenetics, optical fiber implantation was performed after viral injection in the same surgery. Optical fibers (core diameter, 200 μm; length, 5 mm; NA, 0.22; Inper Corporation) were implanted bilaterally and placed 200 μm above the NAc or VP. For *in vivo* fiber photometry, optical fiber implantation was also performed after viral injection in the same surgery. Optical fibers (core diameter, 200 μm; length, 5 mm; NA, 0.37; Inper Corporation) were placed unilaterally in the BLA or VP. A metal head-bar (for head restraint in all mice used in the photometry and behavioral experiments) was subsequently mounted onto the skull with black dental cement. We waited for a minimum of 3-4 weeks before starting the behavioral experiments in these mice.

To trace the cholinergic inputs from the basal forebrain to the BLA, we unilaterally injected 200 nl Cholera Toxin Subunit B, Alexa Fluor™ 555 Conjugate (CTB555; Thermo Fisher Scientific) solution (0.1% in PBS) into the BLA (coordinates: AP -1.7, ML 3.4, and DV -4.6). Coronal brain sections were prepared 5 days after the injection for histological examination of the CTB555-labeled neurons in the basal forebrain. To quantify CTB-labeled cholinergic neurons in the anterior VP and posterior VP, we used the anterior commissure, posterior (acp) a reference. We defined the portion of the VP below the acp as the posterior VP. The coordinates of the posterior VP are roughly +0.38 mm to -0.8 mm from Bregma. The substantia innominata was included in the posterior VP for analysis. The coordinates of the anterior VP are roughly +0.74 mm to +0.38 mm from Bregma. The boundary of the nucleus basalis of Meynert (NBM) is based on the definition by the Paxinos Atlas: the cholinergic cells of the NBM straddle the border between the globus pallidus and the internal capsule.

Immunohistochemistry

Immunohistochemistry experiments were performed following standard procedures described previously.[18,42] Briefly, mice were anesthetized with Euthasol (0.2 ml; Virbac, Fort Worth, Texas, USA) and transcardially perfused with 30 ml PBS, followed by 30 ml 4% paraformaldehyde (PFA) in PBS. Brains were extracted and further fixed in 4% PFA overnight followed by cryoprotection in a 30% PBS-buffered sucrose solution for 36-48 h at 4 °C. Coronal sections (50 μm) were cut using a freezing microtome (Leica SM 2010R, Leica). Sections were first washed in PBS (5 min), incubated in PBST (0.3% Triton X-100 in PBS) for 30 min at room temperature (RT) and then washed with PBS (3 x 5 min). Next, sections were blocked in 5% normal goat serum in PBST for 30 min at RT and then incubated with primary antibodies overnight at 4 °C. Sections were washed with PBS (3 x 5 min) and incubated with fluorescent secondary antibodies at RT for 2 h. In some experiments (as indicated in Figures 1, 2, 3, 4, 5, 6, 7, and S1–S18), sections were washed twice in PBS, incubated with DAPI (4′,6-diamidino-2-phenylindole, Invitrogen, catalogue number D1306) (0.5μg/ml in PBS) for 2 min. After washing with PBS (3 x 5 min), sections were mounted onto slides with Fluoromount-G (eBioscience, San Diego, California, USA). Images were taken using an LSM 780 laser-scanning confocal microscope (Carl Zeiss, Oberkochen, Germany). The primary antibodies used were: chicken anti-GFP (Aves Labs, catalogue number GFP1020; dilution 1:1000), rabbit anti-RFP (Rockland, catalogue number 600-401-379; dilution 1:1000), Anti-choline acetyltransferase (ChAT) antibody (Sigma-Aldrich, catalogue number AB144P; dilution 1:1000). Appropriate fluorophore-conjugated secondary antibodies (Life Technologies) were used depending on the desired fluorescence colors.

Fluorescence *in situ* hybridization

Single-molecule fluorescent *in situ* hybridization (smFISH) (RNAscope, ACDBio) was used to detect the expression of *Pdyn*, *mCherry*, *GFP*, *Oprk1*, *Gad2*, *Tshz1*, *Drd1*, *Drd2*, *tdTomato*, *Vglut2* and *ChAT*. For tissue preparation, mice were first anesthetized with isoflurane and then decapitated. Their brain tissue was first embedded in cryomolds (Sakura Finetek, Catalog number 4566) filled with M-1 Embedding Matrix (Thermo Scientific, Catalog number 1310) and then quickly fresh-frozen on dry ice. The tissue was stored at −80 °C until it was sectioned with a cryostat. Cryostat-cut sections (16-μm thick) containing the brain areas of interest were collected along the rostro- caudal axis in a series of four slides and quickly stored at −80 °C until being processed. Hybridization was carried out using RNAscope kit (ACDBio). On the day of the experiment, frozen sections were postfixed in 4% PFA in RNA-free PBS (hereafter referred to as PBS) at room temperature (RT) for 15 min, then washed in PBS, dehydrated using increasing concentrations of ethanol in water (50%, once; 70%, once; 100%, twice; 5 min each). Sections were then dried at RT and incubated with Protease IV for 30 min at RT. Sections were washed in PBS three times (5 min each) at RT and hybridized.

Probes against *Pdyn* (Catalog number 318771-C2, dilution 1:50), *mCherry* (Catalog number 431201-C3, dilution 1:50), *GFP* (Catalog number 400281-C2, dilution 1:50), *Oprk1* (Catalog number 316111-C1, dilution 1:50), *Gad2* (Catalog number 439371-C2 and C3, dilution 1:50), *Tshz1* (Catalog number 494291-C3, dilution 1:50), *Drd1* (Catalog number 406491-C1, dilution 1:50), *Drd2* (Catalog number 406501-C3, dilution 1:50), *slc17a6* (Catalog number 319171-C3, dilution 1:50), *tdTomato* (Catalog number 317041-C1, dilution 1:50), and *ChAT* (Catalog number 410071-C3, dilution 1:50) were applied to the brain sections. Hybridization was carried out for 2 h at 40 °C. After that, the sections were washed twice in 1× Wash Buffer (Catalog number 310091; 2 min each) at RT, and then incubated with the amplification reagents for three consecutive rounds (30 min, 15 min and 30 min, at 40 °C). After each amplification step, the sections were washed twice in 1× Wash Buffer (2 min each) at RT. Finally, fluorescence detection was carried out for 15 min at 40 °C. Sections were then washed twice in 1× Wash Buffer (2 min each), incubated with DAPI for 2 min, washed twice in 1× Wash Buffer (2 min each), and then mounted with a coverslip using mounting medium.

Images were acquired using an LSM780 confocal microscope equipped with 20x and 40x lenses and visualized and processed using ImageJ and Adobe Illustrator. Cell counting and mean fluorescence intensity quantification of images were performed using ImageJ. To compare gene deletion or knockdown efficiency, brain sections were imaged with the same imaging settings and the fluorescence intensities of targeted genes in the experimental groups were normalized to those of the control groups.

In vitro electrophysiology

Patch-clamp recording was performed as described previously.[62,69] Adult (8- to 16-week-old) mice were deeply anesthetized by an overdose of isoflurane. Their brains were extracted, and coronal brain slices (290 μm thick) were generated at a slicing speed of 0.12 mm/s in ice-cold cutting solution containing 110 mM choline chloride, 25 mM $NaHCO_3$, 1.25 mM NaH_2PO_4, 2.5 mM KCl, 0.5 mM $CaCl_2$, 7.0 mM $MgCl_2$, 25.0 mM glucose, 11.6 mM ascorbic acid and 3.1 mM pyruvic acid (osmolarity, 300-310 mOsm), gassed with 95% O_2 and 5% CO_2 using a vibrating-blade microtome (HM650, Thermo Fisher Scientific). The slices were transferred to a holding chamber and incubated in 34 °C artificial cerebrospinal fluid (ACSF) containing: 118 mM NaCl, 2.5 mM KCl, 26.2 mM $NaHCO_3$, 1 mM NaH_2PO_4, 20 mM glucose, 2 mM $MgCl_2$, and 2 mM $CaCl_2$ (osmolarity, 300-310 mM, pH, 7.4), which was oxygenated with 95% O_2 and 5% CO_2. Forty-five minutes after recovery, the slices were transferred to a recording chamber and perfused with oxygenated ACSF at 3 ml/min at room temperature (20-24 °C).

Whole-cell patch-clamp recordings were performed using glass pipettes with a resistance of 3-7 MΩ. A blue LED (470 nm, pE-100, CoolLED) was used to activate ChR2. The 470-nm light-evoked postsynaptic responses of VP cholinergic neurons were recorded in voltage-clamp mode. The internal solution contained 115 mM cesium methanesulfonate, 20 mM CsCl, 10 mM HEPES, 2.5 mM $MgCl_2$, 4 mM Na_2ATP, 0.4 mM Na_3GTP, 10 mM sodium phosphocreatine and 0.6 mM EGTA (pH 7.2, osmolarity ~295 mOsm). IPSCs were recorded at a voltage of 0 mV. CNQX (10 μM) and D-AP5 (50 μM) was added into the ACSF to block glutamate receptors. Picrotoxin (PTX; 50 μM) was used to block $GABA_A$ receptors. For disinhibition-related experiments, cholinergic or GABAergic neurons in the VP were recorded in current-clamp mode (holding current, 0 pA) using a potassium-based internal solution containing (in mM) 130 K-gluconate, 5 KCl, 2.5 $MgCl_2$, 10 HEPES, 0.6 EGTA, 10 mM sodium phosphocreatine 0.4 Na_3-GTP, and 4 Na_2-ATP (pH 7.2, osmolarity ~290 mOsm). CNQX (10 μM) and D-AP5 (50 μM) was added into the ACSF to block excitatory synaptic inputs. In some experiments, norBNI (nor-Binaltorphimine Dihydrochloride, Sigma-Aldrich, catalogue number 5.08017, 100 nM) was added into the ACSF to block κ-opioid receptors. Action potential firing was obtained every 30 s with light stimulation (a 2-s train of 20-Hz 1-ms light pulses). The locations of VP cholinergic neurons were identified with an air objective (5X; NA 0.10).

Voltage clamp and current clamp recordings were carried out using a MultiClamp 700B amplifier (Molecular Devices). During recording, traces were low-pass filtered at 3 kHz (Digidata 1440A; Molecular Devices). Data were acquired with Axon Clampex 10.2 software. The amplitude of inhibitory postsynaptic currents (IPSCs) was analyzed using pCLAMP 10 and Igor software. IPSC amplitudes were calculated as the difference between the peak amplitude within 50 ms after light stimulation onset and the mean amplitude just before the IPSC. For recording of spontaneous membrane potential and firing rate, cells were held in current clamp mode and no current injections were made. Membrane potential and firing were recorded for at least 2 s before and after light stimulation. Action potential latency was measured as the time difference from the onset of the first light stimulation to the half-height of the peak of the first action potential.

Measuring acetylcholine release in behaving mice

To measure acetylcholine release in response to water and air-puff, custom-built spouts were used to deliver these stimuli to mice. An external trigger from a Bpod State Machine (Sanworks) was used to synchronize the delivery with fiber photometry recording. A water-restriction schedule started 23 h before training. Mice were first habituated in a head-restraint frame for 10 min each day for 2 days. On day 3, mice were trained to lick water from the water spout. Once mice learned to successfully lick water, they were provided with water during fiber photometry recording. In randomly interleaved trials, air-puff was delivered toward the face of the mice. Each session contained 10 trials of water delivery and 10 trials of air-puff delivery. To inhibit NAc^{Pdyn} neurons optogenetically with ArchT and determine the effects of the inhibition on acetylcholine release, a constant green light (532 nm, 10 mW) was delivered into the NAc starting at 50 ms before stimulus (water or air-puff) onset and ending at 100 ms after stimulus (water or air-puff) was ended. Trials with or without the light were randomly interleaved, with inter-trial intervals of 3-7 seconds. There were 10 trials for each trial type (water without light, air-puff without light, water with light, and air-puff with light). To inhibit NAc^{Pdyn} neuron axion terminals optogenetically with PPO and determine the effects of the inhibition on acetylcholine release, a 10-s constant blue light

(470 nm, 10 mW) was delivered into the VP during each inter-trial interval. At 2 s following the cessation of the light, a stimulus (water of air-puff) was delivered to the animal. Trials with or without the light were randomly interleaved, with inter-trial intervals of 21-25 seconds. There were 5 trials for each trial type (water without light, air-puff without light, water with light, and air-puff with light). To activate NAc^{Pdyn} neurons or their axion terminals optogenetically with ChR2 and determine the effects of the activation on acetylcholine release, an external trigger generated by a Bpod State Machine (Sanworks) was used to synchronize the delivery of blue light pulses (470 nm, 5 mW; 50, 100, or 150 ms in duration) into the NAc or VP with fiber photometry recording in the BLA. Each session consisted of 20 trials.

In vivo fiber photometry and data analysis

We used a commercial fiber photometry system (FP3001, Neurophotometrics) to record signals from the dynorphin sensor (klight1.3) and the acetylcholine sensor (gACh3.0; see above "measuring acetylcholine release in behaving mice") *in vivo* in behaving animals under head restraint, through optical fibers (fiber core diameter, 200 μm; fiber length, 5.0 mm; NA, 0.37; Inper) implanted in the VP or BLA. A patch cord (fiber core diameter, 200 μm; Doric Lenses) was used to connect the photometry system with the implanted optical fibers. The intensity of the blue light (λ = 470 nm) for excitation was adjusted to a low level (20–50 μW) at the tip of the patch cord. Emitted sensor fluorescence was bandpass filtered and focused on the sensor of a CCD camera. Photometry signals (frame rate, 20 Hz) and behavioral events were aligned on the basis of an analogue TTL signal generated by the Bpod. Mean values of signals from a region of interest were calculated and saved using Bonsai software (Bonsai) and were exported to MATLAB (2017a) for further analysis. To correct for photobleaching of fluorescence signals (baseline drift), a bi-exponential curve was fitted to the raw fluorescence trace and subtracted as follows:

$$F_{raw\_fit} = \mathrm{fit}(\mathrm{Timestamp}, F_{raw}, \text{'exp 2'})$$

$$F_{raw\_correction} = (F_{raw} - F_{raw\_fit}) / F_{raw\_fit}$$

After baseline drift correction, the fluorescence signals were z-scored relative to the mean and standard deviation of the signals of the entire trace, excluding the time window when laser stimulation occurred (to avoid the light bleed-through from photo-stimulation). Besides the sensor signals, we simultaneously recorded isosbestic signals or mCherry signals which served to monitor potential motion artifacts. Trials with clear motion artifacts were excluded from further analysis.

Go/no-go task

We trained mice in a go/no-go task as previously described.[18] Mice underwent a water-deprivation schedule that started 23 hours before training, and then 2 days of habituation to head restraint. After habituation, mice were trained to lick for water from a metal spout (5 μl per lick, 200 trials per session, 1 session per day for 3 days). Once mice learned to successfully obtain water in at least 85% of the trials, they were subjected to training in the go/no-go task (200 trials per session (100 go trials and 100 no-go trials), 1 session per day). In each trial, a 1-s pure tone cue (the CS) (go cue, 10 kHz, 70 dB; no-go cue, 3 kHz, 70 dB) was presented, followed by a 1-s delay. The delay was designated as the 'decision window'. During go trials, the mice were required to lick at least once during the decision window to receive a drop of water (US; 10 μl), resulting in a hit trial. If mice did not lick during the decision window, they would not receive the water reward, resulting in a miss trial. During no-go trials, if mice licked the spout at least once during the decision window, they would receive a blow (200 ms) of air-puff, resulting in a 'false alarm' (FA) trial. If mice did not lick during the window, they would successfully prevent air-puff delivery, resulting in a 'correct rejection' (CR) trial. Training in this phase persisted until the mice reached a performance level of at least 80% successful trials. The accuracy was calculated as the total correct responses divided by the total trials: accuracy = (hits + correct rejects) / (total trials).

For optogenetic activation, blue light (λ = 470 nm; 5 mW; 20-Hz 5-ms pulses) was delivered during the CS period and decision window. For optogenetic inhibition with PPO, blue light (λ = 470 nm; 10 mW; a 2-s square pulse) was delivered during the CS period and decision window.

For training in the go/no-go task after systemic norBNI application, mice received norBNI (25mg/kg, dissolved in 0.9% saline solution) intraperitoneal (i.p.) injection 3 weeks after they had received virus injection and fiber implantation. The animals were subjected first to fiber photometry recording, both before and 24 hours after the norBNI injection, and subsequently to training in the go/no go task. For training in the go/no-go task after norBNI local application in the VP, mice received norBNI (2.5 mg/ml, 500 nl) injection into the VP 3 weeks after they had received virus injection. Optical fibers were implanted subsequently. One week later, the animals were subjected to fiber photometry measurement. They were subsequently subjected to training in the go/no go task. For training in the go/no-go task after deletion of *Pdyn* or *Oprk1*, mice were subjected to training in the go/no-go task 4 weeks after they had received injection of the virus to delete the respective gene.

Testing the influence of the $NAc^{Pdyn} \rightarrow$ VP projections on licking behavior

For training mice to lick a water spout to obtain water, the mice first underwent a water-deprivation schedule that started 23 h before training, followed by 2 days of habituation to head restraint. These mice were then allowed to obtain water by licking from a metal

spout positioned next to their mouth, just like at the beginning of training in the go/no-go task. To test whether optogenetic activation of $NAc^{Pdyn} \rightarrow VP$ projections could trigger licking in these mice, we delivered blue light pulses (λ = 470 nm, 20 Hz, 5-ms pulse width, 5 mW) into their VP, during which the mice could lick the spout but no water would be delivered. The light pulses were delivered during a 2-s time window in each trial, for a total of 50 trials. The same mice were subsequently allowed to have free access to water. We then repeated the optogenetic stimulation experiment in these mice while they were sated on water.

To test whether optogenetic activation of $NAc^{Pdyn} \rightarrow VP$ projections could trigger licking in naïve mice, we repeated the optogenetic stimulation experiment in water-restricted mice that had never been exposed to the metal spout.

Progressive ratio task

The progressive ratio (PR) task was modified based on a similar task described in a previous study.[42] Water restricted mice were placed in a head-fixed rig equipped with a water port. Mice were first trained to lick into the port for water reward on a ''fixed ratio 1'' (FR1) schedule for 2 days, during which every lick leads to a reward (3 μl of water). Following the FR1 training, the schedule was changed to FR4 for 2 days, which required the mice to lick 4 times with a maximal interlick-interval of 2 minutes in order to receive the reward. Next, the schedule was changed to FR10 for 1 day. Under the FR condition, a session was terminated when the mice had acquired 1 ml of water from the water port, or when the session had lasted for 20 min. Finally, mice were tested with a progressive ratio (PR) schedule in which the number of licks required to obtain one reward followed a geometric progression according to a function:

$$N_j = 20e^{j/20} - 20$$

where j is the trial number. The function was modified on the basis of previous studies.[70,71] Before the PR schedule, mice were tested in an FR10 session. For the optogenetic activation during PR, mice received 20 Hz photo-stimulation (5-ms pulses; 4-s laser on periods with 2-s laser off intervals; power, 5 mW; λ = 473 nm) during the entire PR session (60 min). 24 hours later, the mice were tested again in another PR session (60 min) in the absence of photo-stimulation. For the optogenetic inhibition during PR with PPO, mice received constant blue light (power, 10 mW, λ = 470 nm) during the entire PR session (60 min). 24 hours later, the mice were tested again in another PR session (60 min) in the absence of photo-stimulation.

For training mice in the free-moving PR task, water restricted mice were placed in a chamber equipped with a water port. Mice were first trained to poke into the port for water reward under a FR schedule, same as that in the head-fixed PR task. After the FR schedule (FR1 for 2 days, FR4 for 1 day, and FR10 for 1 day), mice were tested with the PR schedule, same as that in the head-fixed PR task.

Real-time place aversion or preference test

Freely moving mice were initially habituated to a two-sided chamber (23 cm × 33 cm × 25 cm; made from Plexiglas) for 10 min, during which their baseline preference for the left or right side of the chamber was assessed. The test consisted of two sessions (10 min each). During the first session, we assigned one side of the chamber (counterbalanced across mice) as the photo-stimulation side and placed the mice in the non-stimulation side to start the experiment. Once the mouse entered the stimulation side, photo-stimulation (5-ms pulses, 20 Hz, 5 mW measured at the tip of the optic fibers) generated by a 470-nm laser (OEM Laser Systems) was immediately turned on and was turned off as soon as the mouse exited the stimulation side. In the second test session, we repeated this procedure but assigned the other side of the chamber as the stimulation side. The behavior of the mice was recorded with a CCD camera interfaced with Ethovision software (v.11.5; Noldus Information Technologies), which was also used to control the laser stimulation and extract behavioral parameters (position, time, distance, and velocity).

Testing the influence of the $NAc^{Pdyn} \rightarrow VP$ projections on locomotion

We tested the effects of optogenetic activation or inhibition of the $NAc^{Pdyn} \rightarrow VP$ pathway on mice's locomotion in an in an open field in a nontransparent square box (42 × 42 × 40 cm). The arena was enclosed in a sound-attenuating chamber with a house light on the ceiling. Mice were placed in one of the corners of the arena at the start of a session. Locomotion was assessed for 10 min without light stimulation (i.e., ''laser off'') first, then 10 min with light stimulation (i.e., ''laser on''), and lastly another 10 min of laser-off period. For optogenetic activation (with ChR2), the light stimulation was blue (470 nm) light pulses (4-s trains of 20 Hz, 5-ms pulses, separated by 2-s laser-off periods; laser power was 5 mW measured at the tip of the fiber). For optogenetic inhibition (with PPO), the light stimulation was constant blue (470 nm) light, 10 mW measured at the tip of the fiber. Behavior was videotaped, and the resulting data were analyzed using the image processing and tracking software Ethovision XT 5.1 (Noldus Information Technologies).

Elevated plus maze test

The elevated plus maze (EPM) test consisted of a non-transparent, cross-shaped apparatus made of Plexiglass, with two 'closed' arms enclosed by 15-cm-high walls, and two 'open' arms without walls. The arms were 30-cm long and 5-cm wide and extended from a central platform (5 cm × 5 cm), allowing mice to freely move across the arms. The maze was elevated at a height of 55 cm from the ground. At the start of the 10-min sessions, mice were placed in the central platform. Animals' behavior was videotaped, and the resulting data were analyzed using the image processing and tracking software Ethovision XT 5.1 (Noldus Information Technologies).

Behavioral data acquisition and analysis

Behavior experiments were conducted with an open-source platform based on the Bpod State Machine (Sanworks). In the go/no-go task, licking data were acquired by a custom 'lickometer'—a licking detection circuit composed of the metal spout, the mouse, and a ground wire connected to the tail of the mouse. Each time the mice licked the spout, the detection circuit was completed and a lick event was registered. The lick events were recorded by Bpod and saved on a computer. In the go/no-go task, the 'hit' rate was calculated as the number of hit trials divided by the total number of go trials and the 'CR' rate was calculated as the number of CR trials divided by the total number of no-go trials.

QUANTIFICATION AND STATISTICAL ANALYSIS

All statistical tests are indicated where used. Statistical analyses were conducted using GraphPad Prism (v.7; GraphPad Software), MATLAB (2017a) statistical toolbox (MathWorks) and Igor Pro (WaveMetrics). To determine whether parametric tests could be used, the D'Agostino–Pearson test or Shapiro–Wilk test was performed on all data as a test for normality. Parametric tests were used whenever possible to test differences between two or more means. Non-parametric tests were used when data distributions were non-normal. Analysis of variance (ANOVA) was used to check for main effects and interactions in experiments with repeated measures and more than one factor. When main effects or interactions were significant, we performed the planned comparisons according to experimental design (for example, comparing laser on and off conditions). All comparisons were two-tailed. Statistical significance was set at the level of $P < 0.05$. All data are shown as mean ± standard error of the mean (SEM) unless stated otherwise.